Document Number: WATER RESOURCES RESEARCH, VOL. 46, W09527,

Title: Field-scale model for the natural attenuation of uranium at the Hanford 300 Area using high-performance computing

Autjors: Glenn E. Hammond, Peter C. Lichtner

CD provided to
Load in AR

0094239

WATER RESOURCES RESEARCH, VOL. 46, W09527, doi:10.1029/2009WR008819, 2010

RECEIVED
FEB 10 2011
EDMC

Field-scale model for the natural attenuation of uranium at the Hanford 300 Area using high-performance computing

Glenn E. Hammond[1] and Peter C. Lichtner[2]

Received 27 October 2009; revised 6 May 2010; accepted 19 May 2010; published 22 September 2010.

[1] High-resolution, three-dimensional, reactive flow and transport simulations are carried out to describe the migration of hexavalent uranium [U(VI)] at the Hanford 300 Area bordering the Columbia River and to better understand the persistence of the uranium plume at the site. The computer code PFLOTRAN developed under a DOE SciDAC-2 project is employed in the simulations that are executed on ORNL's Cray XT4/XT5 supercomputer Jaguar. The conceptual model used in the simulations is based on the recognition of three distinct phases or time periods in the evolution of the U(VI) plume. These correspond to (1) initial waste emplacement; (2) initial presence of both labile and nonlabile U(VI) with an evolved U(VI) plume extending from the source region to the river boundary, representing present-day conditions; and (3) the complete removal of all nonlabile U(VI) and labile U(VI) in the vadose zone. This work focuses primarily on modeling Phase II using equilibrium and multirate sorption models for labile U(VI) and a continuous source release of nonlabile U(VI) in the South Process Pond through dissolution of metatorbernite as a surrogate mineral. For this case, rapid fluctuations in the Columbia River stage combined with the slow release of nonlabile U(VI) from contaminated sediment are found to play a predominant role in determining the migration behavior of U(VI) with sorption only a second-order effect. Nevertheless, a multirate model was essential in explaining breakthrough curves obtained from laboratory column experiments using the same sediment and is demonstrated to be important in Phase III. The calculations demonstrate that U(VI) is discharged to the river at a highly fluctuating rate in a ratchet-like behavior as the river stage rises and falls. The high-frequency fluctuations must be resolved in the model to calculate the flux of U(VI) at the river boundary. By time averaging the instantaneous flux to average out noise superimposed on the river stage fluctuations, the cumulative U(VI) flux to the river is found to increase approximately linearly with time. The flow rate and U(VI) flux are highly sensitive to the conductance boundary condition that describes the river-sediment interface. By adjusting the conductance coefficient to give a better match to the measured piezometric head, good agreement was obtained with field studies for both the mean flux of water of 10^9 kg/yr and U(VI) of 25 kg/yr at the river-aquifer boundary for a computational domain encompassing the South Process Pond. Finally, it is demonstrated that, through global mass conservation, the U(VI) leach rate from the source region is related to the U(VI) flux at the river boundary.

Citation: Hammond, G. E., and P. C. Lichtner (2010), Field-scale model for the natural attenuation of uranium at the Hanford 300 Area using high-performance computing, *Water Resour. Res.*, *46*, W09527, doi:10.1029/2009WR008819.

1. Introduction

[2] The Hanford 300 Area is located in southeastern Washington State just north of the city of Richland in close proximity to the Columbia River (Figure 1). The site, initially constructed during World War II, was used for research and fabrication of uranium fuel rod assemblies for plutonium production. Large amounts of uranium, copper and other contaminants were disposed of at the site in liquid waste streams. Waste was deposited in two process ponds and in nearby trenches located near the Columbia River. The ponds, referred to as the North (NPP) and South (SPP) Process Ponds, lie near the center of the site approximately 100 m west of the river. Waste streams including U(VI)-Cu (II) and sodium aluminate from the dissolution of spent nuclear fuel and fuel rod cladding were deposited in the ponds and trenches over a period of approximately 32 years from 1943 to 1975. Throughout this period of time, water mounding occurred beneath the ponds dispersing the waste during emplacement. The inventory of waste deposited in the two ponds is estimated as 58,000 kg U, 238,000 kg Cu,

[1]Energy and Environment Directorate, Hydrology Group, Pacific Northwest National Laboratory, Richland, Washington, USA.
[2]Earth and Environmental Sciences Division, Los Alamos National Laboratory, Los Alamos, New Mexico, USA.

Copyright 2010 by the American Geophysical Union.
0043-1397/10/2009WR008819

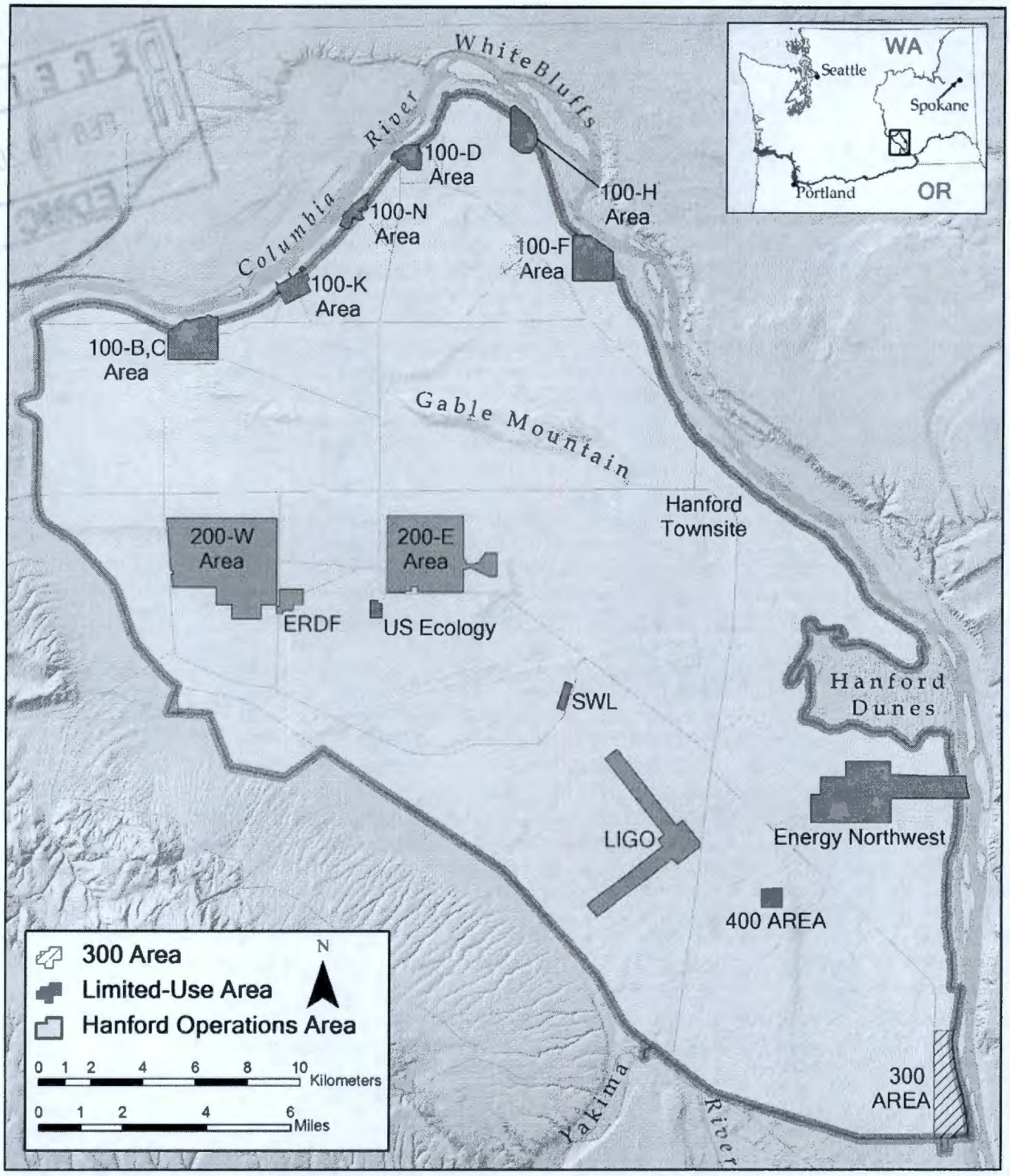

Figure 1. Map of the Hanford Site showing the location of the Hanford 300 Area in the lower right.

1,156,000 kg F, 243,000 kg NO_3^-, and large amounts of Al [*Zachara et al.*, 2005; *Catalano et al.*, 2006]. Smaller undocumented amounts of Ni, Cr, Zn, and P also were deposited. The pH of the pond water varied over time ranging from 1.8 to 11.4. Sodium hydroxide was added to the waste stream when the pH was acidic in an attempt to minimize mobilization of Cu and U through the vadose zone into the underlying unconfined aquifer and subsequently to the Columbia River. Despite removal of highly contaminated pond bottom sediments (>4.2 μmol/g or 1000 ppm U), a groundwater plume of U(VI) with concentrations in excess of 120 μg/L (5.0414×10^{-7} mol/L), or over four times the EPA's maximum contaminant level (MCL) for uranium (i.e., 30 μg/L or 1.26035×10^{-7} mol/L [*Environmental Protection*

Agency, 1998]), has persisted at the Hanford 300 Area [*Zachara et al.*, 2005]. Particularly perplexing are the longevity of the uranium plume at these elevated concentrations and the factors controlling uranium mobility at the site.

[3] One of the first modeling attempts of the Hanford 300 Area was performed by Westinghouse Hanford Corporation using PORFLO-3, a 3-D groundwater flow and contaminant transport code for variably saturated media [*Runchal et al.*, 1992; *Sagar and Runchal*, 1989]. A rectangular 3-D computational domain measuring 3000 m × 2150 m × 30 m was used oriented along the Columbia River. No flow boundary conditions were imposed at the top and bottom of the domain, and time-dependent head conditions at the sides of the domain to account for hourly fluctuations in the river stage. Calculations were carried out for constant K_d values of 0, 1, 10, and 25 cm^3/g. (For an intrinsic sediment density of $\rho_s = 2.65$ g/cm^3 and porosity of 0.3, this is equivalent to a retardation factor of $R = 1 + (1 - \varphi)\rho_s/\varphi = 1$, 7.18, 62.83, and 155.58, respectively.) Variable grid spacing was used ranging from 10 to 65 m horizontally and 1–2 m vertically employing 137,250 nodes. The calculations took approximately 2 cpu hours per year of simulation time on the Hanford Cray computer and were run to a maximum of 26 years from 1992 to 2018. To initialize the calculation, an initial U(VI) plume based on field observations was used in the calculations. The model did not include a continuous source of U(VI), nor was the effect of the Columbia River hyporheic zone on the flow velocity considered. The calculations predicted a maximum flux to the Columbia River of 4.2×10^7 $\mu g/d$, or approximately 15 kg/yr [*DOE*, 1994a, Table 5–4]. In addition, the calculations were consistent with a reduction in the U(VI) concentration in the saturated zone to 20 $\mu g/L$ within 3–10 years [*DOE*, 1994b, p. 4–22]. Based on this and other analyses it was concluded that substantial removal of U(VI) would occur within this time period of 3–10 years [*DOE*, 1994b; *ROD*, 1996] through natural attenuation using a K_d value of 1 cm^3/g. This estimated time period for substantial removal of U(VI) turned out to be highly unrealistic. However, this estimate was contingent on sources within the 300-FF-1 and 300-FF-2 Operable Unit having negligible contributions, or being remediated to protect groundwater [*DOE*, 1994a, p. 5–15; *DOE*, 1994b, p. 5–5].

[4] A constant K_d model cannot account for the slow release of U(VI) as it diffuses along tortuous pathways within sediment grain interiors as a result of mineral dissolution and desorption. A severe limitation of the K_d approach is that it does not account for variable fluid compositions caused by mixing of groundwater and river water, nor does it take into account the impact of changes in sorbed concentrations on retardation. This latter effect can actually lead to a so-called salinity wave that travels unretarded even though the distribution coefficient is nonzero. Differences in dissolved CO_2 and pH between groundwater and river water can result in local changes in sorbed and aqueous U(VI) because of the multicomponent surface complexation reactions. The K_d approach implies a continuous displacement of the center of mass of the U(VI) plume along the direction of flow, with both sorbed and aqueous components advancing in sync at a retarded rate governed by reversible local equilibrium relations. In contrast to the behavior predicted by a K_d model, a solubility- or rate-limited U(VI) source would not be expected to migrate at all. Rather, the source would persist at its original location until all of the U(VI) has been removed by dissolution, desorption, and diffusion. This discussion presupposes that reprecipitation of U(VI) is unlikely given its low concentration. Another difficulty with the K_d approach is accounting for the total U(VI) inventory within a fixed domain. In a K_d model, for a given solution composition, the sorbed concentration is fixed by the value of the distribution coefficient which may not be consistent with the total amount of U(VI) deposited at the site.

[5] One hypothesis for the slower than anticipated release of U(VI) from the sediment is the multiscale nature of the processes involved in leaching U(VI) from the Hanford sediments [*Liu et al.*, 2004, 2006, 2008]. It has been recognized that U(VI) is present in complex, microscopic intergrain fractures, secondary grain coatings, and microporous aggregates [*McKinley et al.*, 2006, 2007], although the precise form of U(VI) in sediments remains elusive. The form of U(VI) in the sediment can be divided into labile and nonlabile components based on the time scale of release, labile being much faster compared to nonlabile. In this work, labile and nonlabile U(VI) are described by sorbed and mineralized forms, respectively.

[6] This study focuses on understanding mobilization and transport of U(VI) in the Hanford 300 Area and in particular the role played by nonlabile U(VI) and rapid fluctuations in the Columbia River stage on the rate of natural attenuation of the U(VI) plume. The primary goal of this study is to better understand the factors controlling the rate of release of U(VI) from the 300 Area site into the Columbia River. Specifically, this study attempts to estimate the present-day rate of attenuation of U(VI) at the site. This goal is far easier to address than the more ambitious question of how long it will take to reduce U(VI) aqueous concentrations to acceptable levels, which requires knowing the present-day in-ground inventory of U(VI), its distribution, and chemical form, all of which are currently uncertain. A measure for the attenuation rate is provided by the cumulative flux of U(VI) into the river integrated over the river-aquifer boundary.

[7] This work is distinguished from the original *DOE* [1994a, 1994b] modeling study, and more recent attempts to model U(VI) migration at the Hanford 300 Area [*Yabusaki et al.*, 2008; *Ma et al.*, 2010], by incorporation of a source term representing both labile and nonlabile U(VI) contained in the vadose and saturated zones, and by incorporation of the low-permeability hyporheic zone through a conductance boundary condition. In this formulation, the time evolution of the system is divided into three phases corresponding to (1) initial waste emplacement, (2) presence of both labile and nonlabile U(VI) with an initial U(VI) plume in place corresponding to present-day conditions, and (3) the absence of all nonlabile forms of U(VI) and labile U(VI) in the vadose zone. This study focuses on the second phase in which the Hanford sediments are equilibrated initially with U(VI) over a region extending from the source region where waste was originally deposited to the Columbia River, corresponding to the plume position for present-day conditions. By contrast, *Yabusaki et al.* [2008] and *Ma et al.* [2010], used a vertical 2-D transport model oriented perpendicular to the river and assumed that the Hanford sediments contain a localized U(VI) source, but otherwise the domain is initially uncontaminated. Nonlabile U(VI) is considered to be inert. There was no attempt in

these studies to model the actual physical system at the Hanford 300 Area and a more schematic approach was used.

[8] In this study, sorption is described through both an equilibrium surface complexation model developed by *Bond et al.* [2008] for the fine-grained fraction of the Hanford sediment, and a multirate model devised by *Liu et al.* [2008]. These authors fit the multirate model to observations of U(VI) breakthrough curves obtained from column experiments containing contaminated fine-grained Hanford sediment. It should be noted that the multirate models employed by *Yabusaki et al.* [2008] and *Liu et al.* [2008], referred to as distributed rate models, differ in that the latter utilized a more mechanistic surface complexation model to describe uranium sorption compared to the extension of the K_d approach used in the former.

[9] In this study, release of nonlabile U(VI) is represented by dissolution of a surrogate mineral from a localized source region at the SPP. Since site characterization is ongoing, site-specific data for the chemical form of the nonlabile U(VI) fraction and its release rate needed to model U(VI) migration at the site is not yet available. However, the model results should in themselves be valuable in aiding the determination of which parameters are most sensitive to predicting U(VI) release from the site and thereby aid in data acquisition.

[10] In what follows, first the governing equations and their numerical discretization and solution are presented in a general context to describe U(VI) attenuation in natural systems with focus on the numerical implementation of a multirate sorption model. The model is applied first to the 1-D small column experiment described by *Liu et al.* [2008] using their multirate sorption model to validate its implementation in PFLOTRAN [*Hammond et al.*, 2008]. Following this, the conceptual model used in this work is described. To setup the 3-D simulations for the Hanford 300 Area, hypothetical 1-D scoping calculations of U(VI) migration are carried out to explore the influence of labile and nonlabile forms of U(VI) on the flux of U(VI) to the river and investigate Phase II and III initial conditions in the model calculations. Finally, results of massively parallel 3-D simulations for Phase II U(VI) migration at the 300 Area are presented. The calculations are executed on Oak Ridge National Laboratory's (ORNL) Cray XT4/XT5 supercomputer Jaguar.

2. Governing Equations

[11] The governing equations that describe quantitatively natural attenuation of U(VI) at the Hanford 300 Area must account for variably saturated flow conditions coupled to chemical reactions involving aqueous speciation, mineral precipitation and dissolution, and sorption through a surface complexation model for both equilibrium and kinetic conditions. The partial differential equations used to describe these processes along with their numerical solution are presented next as implemented in PFLOTRAN.

2.1. Chemical Reactions

[12] The attenuation of U(VI) and its mobility are influenced by various chemical reactions involving aqueous complexation, mineral dissolution and precipitation, and sorption in the form of surface complexation reactions as well as the magnitude and direction of the groundwater flow field. Because of the close placement of the site next to the Columbia River, mixing of river water with groundwater as the river stage rises and falls leads to significantly different concentrations of calcium, carbonate, and pH, which can dramatically affect uranium speciation and thus retardation. For example, in the U(VI) source region the two dominant aqueous U(VI) species are $CaUO_2(CO_3)_3^{2-}$ and $Ca_2UO_2(CO_3)_{3(aq)}$, which together account for over 75% of the total U(VI) in solution.

[13] The reactions taking place in the Hanford groundwater can be formulated in terms of a set of N_c primary species or chemical components $\{\mathcal{A}_j\}$ [*Lichtner*, 1996]. Reactions for homogeneous speciation, mineral precipitation and dissolution, and surface complexation can then be written in the following general forms for homogeneous aqueous complexing reactions:

$$\sum_{j=1}^{N_c} \nu_{ji}^{aq} \mathcal{A}_j \rightleftharpoons \mathcal{A}_i, \tag{1}$$

mineral precipitation/dissolution reactions:

$$\sum_{j=1}^{N_c} \nu_{jm}^{min} \mathcal{A}_j \rightleftharpoons \mathcal{M}_m, \tag{2}$$

and for surface complexation reactions associated with a surface site of type σ:

$$>\mathcal{S}_\sigma + \sum_{j=1}^{N_c} \nu_{ji}^{\sigma} \mathcal{A}_j \rightleftharpoons >\mathcal{S}_{i\sigma}. \tag{3}$$

In these reactions $\mathcal{A}_j$ denotes the jth primary or basis species, $\mathcal{A}_i$ refers to the ith aqueous secondary species, $\mathcal{M}_m$ denotes the mth mineral, and $>\mathcal{S}_{i\sigma}$ refers to the ith surface complex on site σ with empty surface site $>\mathcal{S}_\sigma$. The quantities ν_{ji}^{aq}, ν_{jm}^{min}, and ν_{ji}^{σ}, denote the stoichiometric reaction coefficients for aqueous, mineral, and surface complexation reactions, respectively.

2.1.1. Surface Complexation Model

[14] To implement a surface complexation model for U(VI), site-specific data are needed for the surface site density, selectivity coefficients for the various surface complexes, and identification of the surface complexes themselves to determine the reaction stoichiometry. Bulk properties of the Hanford sediment are used rather than the properties of individual minerals to characterize surface complexation reactions. Sorption is described through a nonelectrostatic, surface complexation model. For conditions of local equilibrium the *Bond et al.* [2008] model is used and for a kinetic description the kinetic multirate model of *Liu et al.* [2008] is used, both derived from sorption experiments with contaminated Hanford sediments. Following *Davis et al.* [1998], protonation-deprotonation reactions are not included because of the excess of surface sites in comparison to U(VI) site occupancy, and the assumption of a nonelectrostatic model. Since protonation-deprotonation reactions involve charged surface complexes ($>SO^-$, $>SOH_2^+$), they would lead to a charge imbalance in the aqueous solution [*Lichtner*, 1996].

[15] For each sorption site σ, the sorbed concentration of surface complexes and empty surface sites satisfy the site conservation equation

$$\omega_\sigma = S_\sigma + \sum_i S_{i\sigma}, \tag{4}$$

involving the sum of concentrations S_σ and $S_{i\sigma}$ corresponding to unoccupied sites and surface complexes, respectively. The site concentration ω_σ [mol sites/m^3] is related to the specific site surface density η_σ [mol sites/m^2] of the medium by the equation

$$\omega_\sigma = \eta_\sigma \mathcal{A}_\sigma \rho_r (1-\varphi). \tag{5}$$

In this equation the quantity η_σ denotes the moles of surface sites of type σ per unit area, $\mathcal{A}_\sigma$ [m^2/kg] represents the specific sorptive surface area, ρ_r [kg/m^3] refers to the rock grain density, and porosity is denoted by φ. Volumetric $S_{i\sigma}$ [mol/m^3] and surface-based $\Gamma_{i\sigma}$ [mol/m^2] sorbed concentrations are related through the porosity, specific surface area, and grain density of the medium according to the expression

$$S_{i\sigma} = \Gamma_{i\sigma} \mathcal{A}_\sigma \rho_r (1-\varphi). \tag{6}$$

2.1.1.1. Equilibrium Surface Complexation Model

[16] The equilibrium concentrations for unoccupied sites S_σ^{eq} and the ith surface complex $S_{i\sigma}^{eq}$ are derived from the mass action equation corresponding to reaction (3) resulting in the expressions

$$S_\sigma^{eq} = \frac{\omega_\sigma}{1+\sum_i K_{i\sigma} Q_{i\sigma}}, \tag{7}$$

and

$$\begin{aligned} S_{i\sigma}^{eq} &= K_{i\sigma} Q_{i\sigma} S_\sigma^{eq}, \\ &= \frac{\omega_\sigma K_{i\sigma} Q_{i\sigma}}{1+\sum_{i'} K_{i'\sigma} Q_{i'\sigma}}, \end{aligned} \tag{8}$$

with selectivity coefficient $K_{i\sigma}$ and surface site concentration ω_σ, where the aqueous ion activity product $Q_{i\sigma}$ is defined by

$$Q_{i\sigma} = \prod_j (\gamma_j C_j)^{\nu_{ji}^\sigma}, \tag{9}$$

with aqueous activity coefficient γ_j and concentration C_j. Accordingly, the sorbed and empty site concentrations are proportional to the bulk surface site concentration ω_σ.

2.1.1.2. Multirate Sorption Model

[17] The multirate sorption model is based on a kinetic formulation of surface complexation derived from the equilibrium model. The kinetic formulation for the rate of reaction (3), assuming it obeys the form of an elementary rate law, can be written as

$$\frac{\partial S_{i\sigma}}{\partial t} = \kappa_{i\sigma}^f Q_{i\sigma} S_\sigma - \kappa_{i\sigma}^b S_{i\sigma}, \tag{10}$$

with forward and backward rate constants $\kappa_{i\sigma}^{f,b}$, their ratio equal to the selectivity coefficient: $K_{i\sigma} = \kappa_{i\sigma}^f / \kappa_{i\sigma}^b$. Factoring out $k_{i\sigma}^b$ allows the rate to be expressed in the form

$$\frac{\partial S_{i\sigma}}{\partial t} = \kappa_{i\sigma}^b (K_{i\sigma} Q_{i\sigma} S_\sigma - S_{i\sigma}). \tag{11}$$

In general, the rate constants vary for different surface complexes, their ratio equal to the selectivity coefficient for the reaction as already noted. In the multirate model, however, it is assumed that the backward rate constant, denoted simply as κ_l, is the same for all surface complexes, but may vary for different physical domains indexed by the subscript l within the porous medium. With each rate constant κ_l may be associated a different site density $\omega_{l\sigma} = f_l \omega_\sigma$ with the site fraction f_l satisfying $\sum_l f_l = 1$. Thus the form of the multirate sorption equations are assumed to be given by

$$\frac{\partial S_{il}^\sigma}{\partial t} = \kappa_l (f_l S_{i\sigma}^{eq} - S_{il}^\sigma), \tag{12}$$

with the equilibrium isotherm $S_{i\sigma}^{eq}$ given by equation (8). The rate constants κ_l are obtained from a probability distribution $\mathcal{P}$, such as Poisson or log normal distributions, according to the relation [*Liu et al.*, 2008]

$$f_l = \int_{\kappa_l - \Delta\kappa_l/2}^{\kappa_l + \Delta\kappa_l/2} \mathcal{P}(\kappa|\alpha,\beta) d\kappa, \tag{13}$$

with mean β and standard deviation α. Thus the distribution in rate constants can be characterized with the independent parameters: $\kappa_l = \kappa_l(f_l, \alpha, \beta)$. In this work following *Liu et al.* [2008] the log normal distribution

$$\mathcal{P}(\kappa|\alpha,\beta) = \frac{1}{\kappa\alpha\sqrt{2\pi}} \exp\left[-\frac{1}{2\alpha^2}(\ln\kappa - \ln\beta)^2\right], \tag{14}$$

is used.

[18] Because the multirate rate constants κ_l are independent of the individual surface complexes, it is equivalent whether one uses the total sorbed concentration defined as

$$S_{jl}^\sigma = \sum_i \nu_{ji}^\sigma S_{il}^\sigma, \tag{15}$$

or the individual surface complex concentrations S_{il}^σ in formulating the kinetic rate equations. Thus equation (12) can be replaced by

$$\frac{\partial S_{jl}^\sigma}{\partial t} = \kappa_l \left(f_l S_{j\sigma}^{eq} - S_{jl}^\sigma\right), \tag{16}$$

with

$$S_{j\sigma}^{eq} = \sum_i \nu_{ji}^\sigma S_{i\sigma}^{eq}. \tag{17}$$

This would not be possible if the rate constants κ_l also depended on the surface complex species $\mathcal{S}_{i\sigma}$. Finally, note that in the limit $\kappa_l \to \infty$, $S_{il}^\sigma \to f_l S_{i\sigma}^{eq}$, and in this limit the local equilibrium sorption isotherm is retrieved from the multirate model.

2.1.2. Mineral Reactions

[19] Mineral reactions are described through a kinetic rate law based on transition state theory with the reaction rate I_m given by

$$I_m = -k_m a_m \mathcal{P}_m [1 - K_m Q_m] \zeta_m(\varphi_m, K_m Q_m), \tag{18}$$

for the mth mineral, where k_m denotes the kinetic rate constant, a_m represents the specific surface area, $\mathcal{P}_m$ denotes a prefactor to account for the dependence of the rate on pH and other species, K_m denotes the equilibrium constant, and Q_m the ion activity product defined by

$$Q_m = \prod_j (\gamma_j C_j)^{\nu_{jm}^{min}}. \tag{19}$$

The factor in square brackets in equation (18), referred to as the affinity factor, gives the extent of disequilibrium of the reaction. The product $k_m a_m$ is referred to as the effective rate

constant. The multiplicative factor ζ_m on the right-hand side of equation (18) takes the values one or zero depending on whether the mineral is present ($\varphi_m > 0$) or supersaturated ($K_m Q_m > 1$), or not present ($\varphi_m = 0$) and undersaturated ($K_m Q_m < 1$), respectively. The reaction rate is taken to be positive for precipitation and negative for dissolution. For far from equilibrium undersaturated conditions ($K_m Q_m \ll 1$), the rate reduces to the expression

$$I_m = -k_m a_m \mathcal{P}_m, \tag{20}$$

and becomes independent of concentration in the absence of the prefactor $\mathcal{P}_m$.

2.2. Mass Conservation Equations

[20] The governing equations for reactive flow and transport coupled to reactions (1), (2) and (3) in variably saturated porous media are detailed below. The flow and transport equations are solved sequentially, with saturation state and velocity field passed from the flow to the transport equations at each time step. Because of the relatively short time spans considered (~1 year), there is negligible change in porosity and permeability due to reaction. The flow equations based on Richards equation have the form

$$\frac{\partial}{\partial t}(\varphi s \rho) + \nabla \cdot \rho \mathbf{q} = 0, \tag{21}$$

with water density ρ, porosity φ, and saturation s. The Darcy velocity $\boldsymbol{q}$ is given by

$$\boldsymbol{q} = -\frac{k k_r}{\mu} \nabla (p - \rho g \mathbf{z}), \tag{22}$$

with water pressure p, viscosity μ, acceleration of gravity g, intrinsic permeability k, and relative permeability k_r a function of saturation. The van Genuchten relation is used to relate capillary pressure to water saturation and the Burdine correlation is used for relative permeability.

[21] With the Richards approximation, interaction with the gas phase is neglected resulting in a simplified form for the reactive solute equations that only involves aqueous species. Because uranium is in the VI valence state oxidation does not occur and the Richards equation is a satisfactory approximation. With this simplification the multicomponent reactive transport equations in variably saturated porous media have the form [*Lichtner*, 1996]

$$\frac{\partial}{\partial t}\left(\varphi s \Psi_j + \sum_{\sigma l} S_{jl}^{\sigma}\right) + \nabla \cdot \Omega_j = -\sum_m \nu_{jm}^{\min} I_m, \tag{23}$$

involving only the aqueous phase. In this equation the quantity Ψ_j denotes the total aqueous concentration of the jth primary species given by

$$\Psi_j = C_j + \sum_i \nu_{ji}^{aq} C_i, \tag{24}$$

where the concentration of the ith secondary species is a function of the primary species activities through the mass action relation

$$C_i = \frac{K_i}{\gamma_i} \prod_j (\gamma_j C_j)^{\nu_{ji}^{aq}}, \tag{25}$$

corresponding to reaction (1), with equilibrium constant K_i and activity coefficients $\gamma_{i,j}$. The solute flux $\boldsymbol{\Omega}_j$ is defined by

$$\boldsymbol{\Omega}_j = (\boldsymbol{q} - \varphi s D \nabla)\Psi_j, \tag{26}$$

with diffusion/dispersion coefficient D. The Darcy velocity $\boldsymbol{q}$ and water saturation s are obtained from solving the flow equations. The form of the flux in equation (26) follows if diffusion coefficients are assumed to be species independent. The sorbed concentration S_{jl}^{σ} is obtained by solving the kinetic multirate equation given by equation (16), or may refer to the equilibrium sorption isotherm (in which case S_{jl}^{σ} is replaced by $S_{j\sigma}^{eq}$).

[22] Attenuation of the nonlabile form of U(VI) as well as changes in the amounts of other minerals such as calcite is described through the mass transfer equation

$$\frac{\partial \varphi_m}{\partial t} = \overline{V}_m I_m, \tag{27}$$

which determines the amount of each mineral that has dissolved or precipitated. In this equation $\overline{V}$ and φ_m refer to the mineral molar volume and volume fraction, respectively. Porosity is coupled to changes in mineral volume fraction through the relation

$$\varphi = 1 - \sum_m \varphi_m, \tag{28}$$

under the assumption that reaction only affects the connected porosity. However, for the short time scales encountered in this work porosity may be assumed constant without any loss in generality.

2.3. Local Retardation Factor

[23] A rough indication of the U(VI) mobility is provided by the locally evaluated dimensionless distribution coefficient $\mathcal{K}_j^D$ defined as

$$\mathcal{K}_j^D = \frac{1}{\varphi s \Psi_j} \sum_{\sigma l} S_{jl}^{\sigma}. \tag{29}$$

The dimensioned form of the distribution coefficient K_j^D with units m^3/kg, is related to the dimensionless form according to

$$\mathcal{K}_j^D = \frac{(1-\varphi)}{\varphi s} \rho_s K_j^D, \tag{30}$$

with solid grain density ρ_s. Introducing the distribution coefficient into the solute transport equations yields

$$\frac{\partial}{\partial t}(\varphi s \mathcal{R}_j \Psi_j) + \nabla \cdot \boldsymbol{\Omega}_j = -\sum_m \nu_{jm}^{\min} I_m. \tag{31}$$

with retardation factor $\mathcal{R}_j$ defined as

$$\mathcal{R}_j = 1 + \mathcal{K}_j^D. \tag{32}$$

In general $\mathcal{R}_j$ is not constant and therefore cannot be taken outside the time derivative on the left-hand side of this equation. In fact, simulations presented below show that $\mathcal{R}_j$ for U(VI) is highly variable both temporally and spatially and changes with the direction of flow.

2.4. Numerical Implementation

[24] Calculations are carried out using the massively parallel code PFLOTRAN [*Hammond et al.*, 2008]. PFLOTRAN is an object-oriented reactive multiphase flow and multicomponent geochemical transport code written in Fortran9X. The code is founded upon established and well-supported frameworks for high-performance computing (i.e., PETSc, SAMRAI, MPI, HDF5) and employs domain decomposition to distribute a problem domain across multiple processor cores. PFLOTRAN is designed for execution on a variety of computer architectures from laptops to leadership class supercomputers. The code has employed as many as 131,072 cores on Jaguar, the massively parallel Cray XT4/XT5 at ORNL, for problems composed of up to 2 billion degrees of freedom. Further details of the code and its parallelization are presented by G. E. Hammond et al. (PFLOTRAN: Reactive flow and transport code for use on laptops to leadership-class supercomputers, Bentham E-book, submitted for publication, 2010). Finite volume techniques are used to discretize the flow and transport partial differential equations on a structured grid. Use of a structured grid requires inactive cells at irregular boundaries representing the river and ground surface. A fully implicit backward Euler approach with upwinding is used with sequential coupling between flow and transport modes.

[25] The residual equation for flow has the finite volume discretized form

$$R_n^{(k+1)} = \frac{(\varphi\rho)_n^{(k+1)} - (\varphi\rho)_n^{(k)}}{\Delta t_k} + \frac{1}{V_n}\sum_{n'} A_{nn'}F_{nn'}^{(k+1)} = 0, \quad (33)$$

for the $k+1$st time step with variable time step size $\Delta t_k = t_{k+1} - t_k$, where the sum n' is over all control volumes connected to the nth node with volume V_n and interfacial area $A_{nn'}$. The discretized flux F_{nn} at the interface $n - n'$ between nodes n and n' has the following form

$$F_{nn'} = -\rho_{nn'}\left(\frac{kk_r}{\mu}\right)_{nn'}\left[\frac{P_{n'} - P_n - \rho_{nn'}gz_{nn'}}{d_{n'} + d_n}\right], \quad (34)$$

where the quantities in brackets $()_{nn'}$ are calculated at the interface using a harmonic mean for permeability k, and upstream weighting for the mobility k_r/μ. The density $\rho_{nn'}$ is computed using an arithmetic mean. At the Columbia River boundary a conductance boundary condition is imposed to dampen the river stage fluctuations. At an exterior face b of the boundary cell n, the boundary flux is given by

$$F_{nb} = -\rho_{nb}\left(\frac{kk_r}{\mu}\right)_{nb}\left[\frac{P_b - P_n - \rho_{nb}gz_{nb}}{d_{nb}}\right], \quad (35)$$

where P_b and P_n are the pressures at the face and cell center, respectively, and d_{nb} is the distance between the face and cell center. The permeability at the river boundary is set to the value

$$k_{nb} = Cd_{nb}, \quad (36)$$

where the quantity C is referred to as the boundary conductance coefficient.

[26] The residual equations for reactive transport have the discretized form

$$R_{jn}^{(k+1)} = \frac{(\varphi s\Psi_j)_n^{(k+1)} - (\varphi s\Psi_j)_n^{(k)}}{\Delta t_k} + \sum_{\sigma l}\frac{S_{jln}^{\sigma,(k+1)} - S_{jln}^{\sigma,(k)}}{\Delta t_k} + \frac{1}{V_n}\sum_{n'} A_{nn'}\Omega_{jnn'}^{(k+1)} - \sum_m \nu_{jm}^{\min} I_{mn}^{(k+1)} = 0. \quad (37)$$

The surface complex concentration in the multirate model is obtained by solving the kinetic equation (16). Combined with the N_c primary species, N_{srf} surface complexes for a single sorption site, and M kinetic rate constants, there are $N_{\mathrm{srf}} \times M$ surface complex concentrations giving a total of $N_{\mathrm{dof}} = N_c + N_{\mathrm{srf}} \times M$ unknown quantities for each control volume. For $N_c = 15$, $N_{\mathrm{srf}} = 2$, and $M = 50$, this would give $N_{\mathrm{dof}} = 115$ degrees of freedom per spatial node, resulting in a significant increase in computational effort.

[27] Fortunately, the resulting system of equations can be greatly simplified by eliminating the sorbed concentrations $S_{jl}^{\sigma,(k+1)}$ from the transport equations. Writing a fully implicit backward Euler finite difference form of equation (16) at each node as

$$\frac{S_{jl}^{\sigma,(k+1)} - S_{jl}^{\sigma,(k)}}{\Delta t} = \kappa_l\left(f_l S_{j\sigma}^{\mathrm{eq},(k+1)} - S_{jl}^{\sigma,(k+1)}\right), \quad (38)$$

and solving equation (38) for $S_{jl}^{\sigma,(k+1)}$ gives

$$S_{jl}^{\sigma,(k+1)} = \frac{S_{jl}^{\sigma,(k)} + \kappa_l\Delta t f_l S_{j\sigma}^{\mathrm{eq},(k+1)}}{1 + \kappa_l\Delta t}. \quad (39)$$

With this relation the sorbed concentration variables $S_{jl}^{\sigma,(k+1)}$ can be eliminated from the solute transport equations. The implicit discretization is unconditionally stable as can be seen in the limit $\kappa_l\Delta t \gg 1$, for which $S_{jl}^{\sigma,(k+1)} \to f_l S_{j\sigma}^{\mathrm{eq},(k+1)}$, leading to the condition of local equilibrium.

[28] With the explicit expression for $S_{jl}^{\sigma,(k+1)}$ given in equation (39), it follows from equation (38) that

$$\frac{\partial S_{jl}^{\sigma}}{\partial t} \simeq \frac{\kappa_l}{1 + \kappa_l\Delta t}\left(f_l S_{j\sigma}^{\mathrm{eq},(k+1)} - S_{jl}^{\sigma,(k)}\right), \quad (40)$$

and substituting this result into the primary species transport equations yields a set of algebraic equations which do not involve the unknown sorbed concentrations $S_{il}^{\sigma,(k+1)}$

$$R_{jn}^{j+1} = \frac{(\varphi s\Psi_j)_n^{(k+1)} - (\varphi s\Psi_j)_n^{(k)}}{\Delta t} + \sum_{l\sigma}\frac{\kappa_l}{1 + \kappa_l\Delta t}\left(f_l S_{j\sigma}^{\mathrm{eq},(k+1)} - S_{jl}^{\sigma,(k)}\right) + \frac{1}{V_n}\sum_{n'} A_{nn'}\Omega_{jnn'}^{(k+1)} + \sum_m \nu_{jm}^{\min} I_{mn}^{(k+1)}. \quad (41)$$

The equilibrium sorbed concentration $S_{j\sigma}^{\mathrm{eq},(k+1)}$ is a known nonlinear function of the primary species concentrations at the new time level given by equation (8). Equation (41) can now be solved for the N_c primary species concentrations. Once these equations are solved the sorbed concentrations are obtained directly from equation (39). Thus the full system of $(N_c + N_{\mathrm{srf}} \times M) \times N$ equations, where N refers to the number of spatial nodes, is reduced to solving $N_c \times N$ primary species equations. The governing finite volume

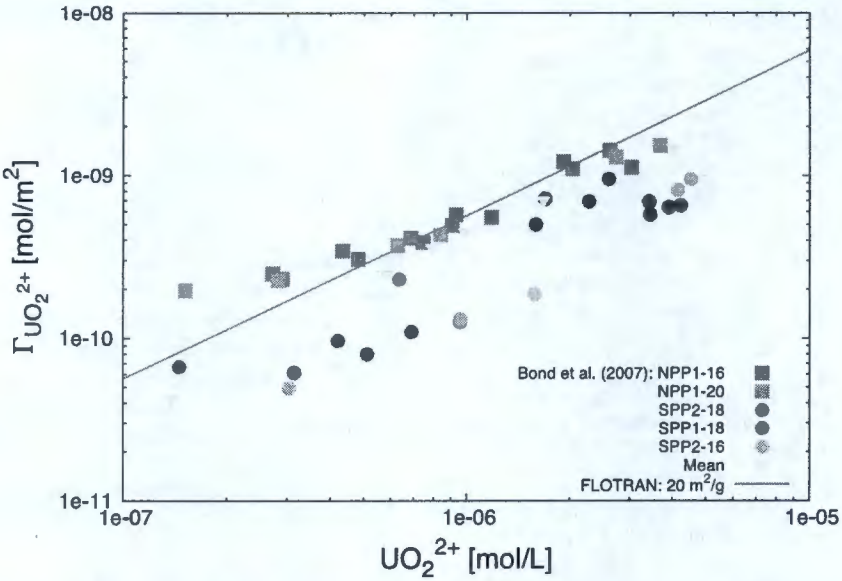

Figure 2. Sorption isotherm for U(VI) with selectivity coefficients and data taken from *Bond et al.* [2008]. To obtain the model result, the relation $\Gamma_{U(VI)} = S_{U(VI)}/(A\rho_r(1 - \varphi))$ is used with specific surface area $A = 20$ m^2/g, grain density $\rho_r = 2.65$ g/cm^3, porosity $\varphi = 0.25$, and a surface site density $\Gamma_A = 3.84$ μmol/m^2. PFLOTRAN results are based on the selectivity coefficients obtained from fitting simultaneously both NPP and SPP data sets [*Bond et al.*, 2008].

equations (33) and (41) may be solved on a single processor or on multiple processor cores using PFLOTRAN.

3. Small Column Experiment

[29] To validate implementation of the multirate kinetic sorption model used in PFLOTRAN and to further investigate the relations between multirate and equilibrium sorption models, in this section PFLOTRAN is applied to the 1-D column experiment analyzed by *Liu et al.* [2008]. This experiment was originally designed to help explain the slow removal of U(VI) from the Hanford 300 Area through kinetically limited desorption of U(VI) from the Hanford sediment. However, the experiment was based on unidirectional flow and did not account for the high-frequency oscillations in the Columbia River stage which, as demonstrated below, play a key role in the attenuation rate of U(VI) at the site. The column, 10.5 cm long, contained <2 mm Hanford sediment grain size fraction. The *Liu et al.* [2008] model is based on the equilibrium surface complexation reactions developed by *Bond et al.* [2008] for the Hanford sediment with minor modifications to the surface complex selectivity coefficients. The surface density of sorption sites used in the simulations is taken from *Bond et al.* [2008] with the value $\eta = 3.84$ μmol/m^2. Using a rock density $\rho_r = 2.65$g/cm^3, porosity $\varphi = 0.25$, and specific surface area $\mathcal{A} = 20$ m^2/g (*Bond et al.* [2008] report average surface areas for NPP = 20.4 m^2/g and SPP = 19.1 m^2/g), gives for the volumetric site density $\omega = 152.64$ mol/m^3, according to equations (5) and (6). A comparison between the equilibrium model and data from *Bond et al.* [2008] is shown in Figure 2. Note that only a small fraction (<1%) of the sorption sites are occupied with U(VI).

[30] The rate constants employed in the multirate model are the same as used by *Liu et al.* [2008], who fit the multirate model to breakthrough curves obtained from the 1-D small column experiment employing stop-flow events with a Darcy flow velocity of 3.25 cm/h with a porosity of 0.41 as described in detail by *Liu et al.* [2008]. Following *Liu et al.* [2008] a total of $M = 50$ rate constants are used obtained from a log normal distribution for the rate constants. Parameters obtained for the log normal distribution for the rates were mean $\beta = 10^{-4.325}$ h^{-1} and standard deviation $\alpha = 2.68$ h^{-1}.

[31] Results comparing the multirate surface complexation model to the experimental breakthrough curves with and without calcite present are depicted in Figure 3, including magnification of each flow period. An effective rate constant of 10^{-12} mol/cm^3/s for calcite is used in the simulation. Although a site-specific value has not been measured, this value was chosen to lie between transport and surface controlled reaction. Chemical reactions for the dominant uranium-bearing aqueous complexes in the simulation are listed in Table 1, and the uranium surface complexes and minerals are listed in Table 2. Shown are both the U(VI) breakthrough curve and the concentration during stopped flow conditions at the end of the column. Although significant variation in U(VI) concentration occurs with and without calcite during periods of no flow, this appears to have little effect on the U(VI) breakthrough curve. The greatest discrepancy between the model results and the experiment occurs at the onset of flow. It is also noted that the calculated peak concentrations using PFLOTRAN appear to be somewhat higher than the values obtained by *Liu et al.* [2008].

[32] Shown in Figure 4 is a comparison between no sorption, equilibrium and multirate model breakthrough curves for the 1-D column experiment with calcite present over long time spans, extrapolating beyond the experiment. The case without sorption leaches out U(VI) most rapidly

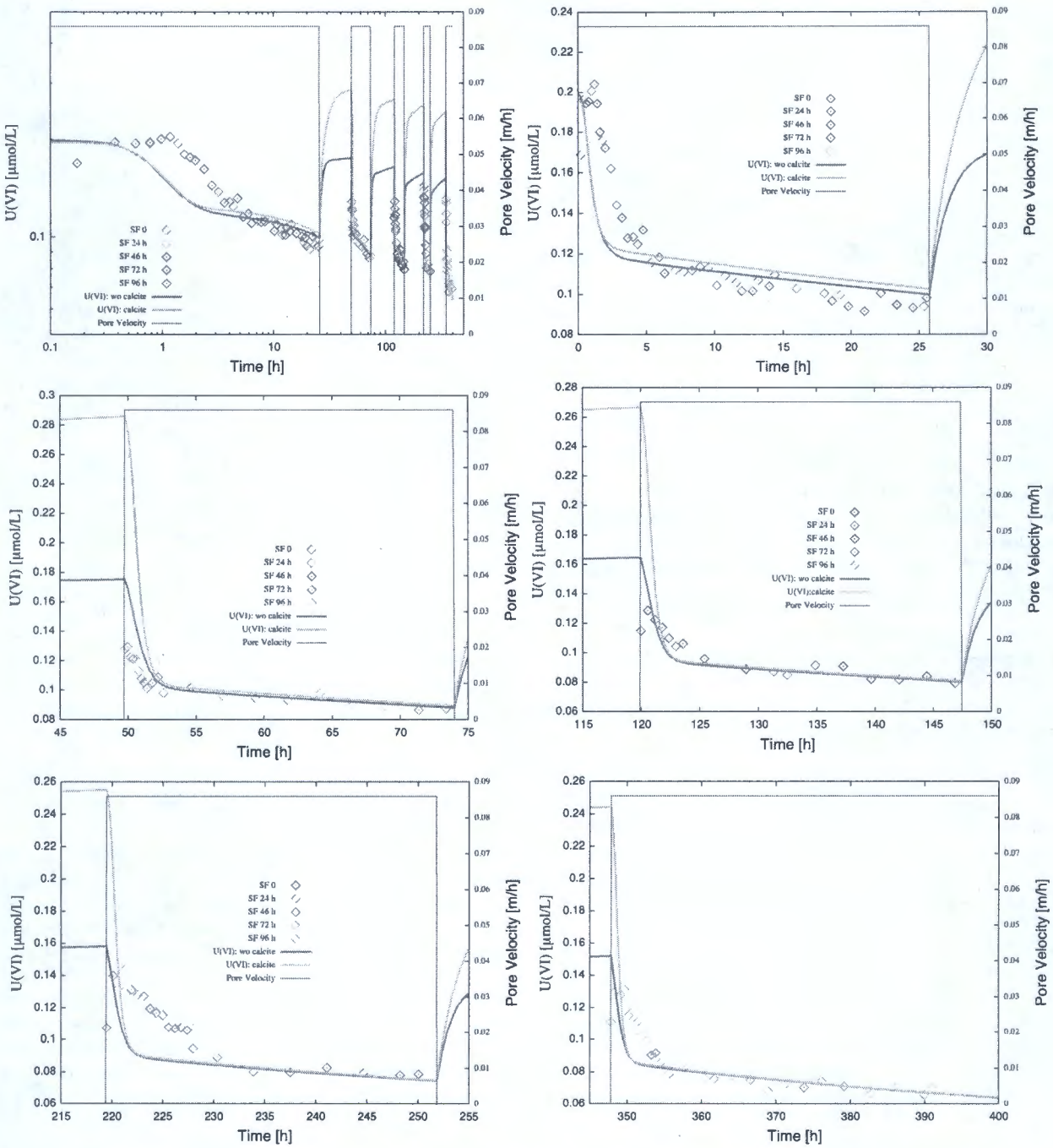

Figure 3. Comparison of breakthrough curves calculated using PFLOTRAN with the multirate sorption model employing rate constants provided by *Liu et al.* [2008] with the small column stop-flow experiment (symbols) discussed by *Liu et al.* [2008], with and without calcite present. Also shown is the U(VI) concentration during stopped flow at the end of the column. The step-function curve indicates periods of flow.

because U(VI) is contained only within the saturated pore volume and not in the solid. The equilibrium sorption model yields higher U(VI) concentrations as a result of its faster desorption rate compared to the multirate model. For earlier times, the multirate breakthrough curve is bracketed by the equilibrium and no sorption curves. However, after very long times the breakthrough curves eventually cross. This is because the equilibrium model results in faster depletion of U(VI) from the sediment compared to the multirate model. By multiplying the multirate kinetic constants by a sufficiently large-scale factor the equilibrium sorption result is obtained, although it should be noted that the scaled rate constants cannot be derived from a log normal distribution in contrast to the unscaled rates. The close agreement with the results obtained by *Liu et al.* [2008] and the correct limiting form of the multirate model approaching local

Table 1. Reactions and Equilibrium Constants for Dominant Aqueous U(VI) Species Used in This Study[a]

Aqueous Reactions	log$K$
$UO_2(OH)_{2(aq)} \rightleftharpoons UO_2^{2+} - 2\ H^+ + 2\ H_2O$	10.3150
$UO_2CO_{3(aq)} \rightleftharpoons UO_2^{2+} + HCO_3^- - H^+$	0.6634
$UO_2(CO_3)_2^{2-} \rightleftharpoons UO_2^{2+} + 2\ HCO_3^- - 2\ H^+$	3.7467
$UO_2(CO_3)_3^{4-} \rightleftharpoons UO_2^{2+} + 3\ HCO_3^- - 3\ H^+$	9.4302
$CaUO_2(CO_3)_3^{2-} \rightleftharpoons Ca^{2+} + UO_2^{2+} + 3\ HCO_3^- - 3\ H^+$	5.3464
$Ca_2UO_2(CO_3)_{3(aq)} \rightleftharpoons 2\ Ca^{2+} + UO_2^{2+} + 3\ HCO_3^- - 3\ H^+$	0.9464

[a]Thermodynamic data are taken from *Guillaumount et al.* [2003] with the exception of the two Ca-U-CO_3 species, which were taken from *Dong and Brooks* [2006].

equilibrium provides validation of the PFLOTRAN implementation of the kinetic model.

4. Conceptual Model

[33] A quantitative description of flow and reactive transport at the Hanford 300 Area is complicated by the highly permeable Hanford Unit, the uppermost rock/soil layer in the unconfined aquifer, and the rapid fluctuating elevation in the Columbia River stage which produces changes in magnitude and direction of flow on an hourly basis, as shown in Figure 5. The insert shows fluctuations over periods of tens of hours or less.

[34] Diurnal fluctuations in river stage can be up to 1.5 meters, while seasonal fluctuations can exceed 2.5 meters. The variable release of water from Priest Rapids Dam upriver is the cause of diurnal fluctuations, while seasonal variations are due to rain fall, snowmelt, and irrigation. The fluctuation in river stage along with the highly permeable Hanford Unit causes river water to flow into the contaminated area during high stage and retreat during low stage. These fluctuations directly impact the water table beneath the Hanford 300 Area resulting in the release of U(VI) through desorption and dissolution processes from the vadose zone. The migration of U(VI) at the site is a complex process very likely involving a continuous source both from the vadose and saturated zones combined with a rapidly oscillating magnitude and direction in flow to and from the river.

4.1. Estimate of Time to Completely Remove U(VI)

[35] The inadequacy of a K_d approach becomes apparent in a simple estimate of the time needed to remove all uranium contained in sediment from the Hanford 300 Area assuming all solid phase U(VI) is in its labile reversibly reacting sorbed form. From the 3-D simulations presented below (see section 5), the mean Darcy velocity obtained for flow to the Columbia River is approximately 80 m/yr with a retardation factor for U(VI) for flow in the direction of the river of approximately 50. With a porosity of $\varphi \simeq 20\%$ and maximum travel distance of approximately $l \simeq 200$ m from the primary U(VI) source region located at the SPP to the river, this gives for the time τ for the uranium plume to reach the river the approximate value

$$\tau = \frac{\varphi \mathcal{R} l}{q} \simeq \frac{0.2 \times 50 \times 200}{80} \text{years} = 25 \text{ years}. \qquad (42)$$

Clearly this estimate is far too short contradicting present-day observations of a large source of uranium remaining on site after an elapsed time of over 35 years since emplacement of waste ceased. A major question then is, what process or processes are prolonging the displacement of uranium from the 300 Area? To address this question, the conceptual model for quantitatively modeling U(VI) migration at the site is introduced in the next section.

4.2. Choice of Initial Conditions: Three Distinct Modeling Phases

[36] To set up a model to describe migration of the U(VI) at the Hanford site it is necessary to specify the initial conditions that are to be imposed on the model corresponding to $t = 0$. The most obvious and easily implemented initial condition is simply to assume uncontaminated conditions before U(VI) and other waste products were first deposited at the site in 1943. This, however, is problematic because the composition and variability of the waste stream over time and its rate of deposition is largely unknown and would be impossible to accurately reconstruct from historical records. In addition, it would seem difficult to develop models that could account for the intergranular deposition of U(VI) on mineral surfaces

Table 2. Reactions and Equilibrium Constants for Minerals and Surface Complexation Reactions Used in This Study[a]

Mineral Reactions	log$K$
$Ca^{2+} + HCO_3^- - H^+ \rightleftharpoons CaCO_{3(s)}$	1.8487[b]
$Cu^{2+} + 2\ UO_2^{2+} + 2\ HPO_4^{2-} + 8\ H_2O - 2\ H^+ \rightleftharpoons$ Metatorbernite	−31[c]
Surface Complexation Reactions	**Selectivity Coefficient**
$>SOH + UO_2^{2+} - 2\ H^+ + H_2O \rightleftharpoons >SOUO_2OH$	−5.152
$>SOH + UO_2^{2+} - 2\ H^+ + CO_{2(aq)} + H_2O \rightleftharpoons >SOHUO_2CO_3$	−0.833

[a]Surface complex selectivity coefficients are taken from *Bond et al.* [2008].
[b]*Plummer and Busenberg* [1982].
[c]See text for explanation. More recently, *Ilton et al.* [2010] have obtained the value log$K$ = −28 for metatorbernite.

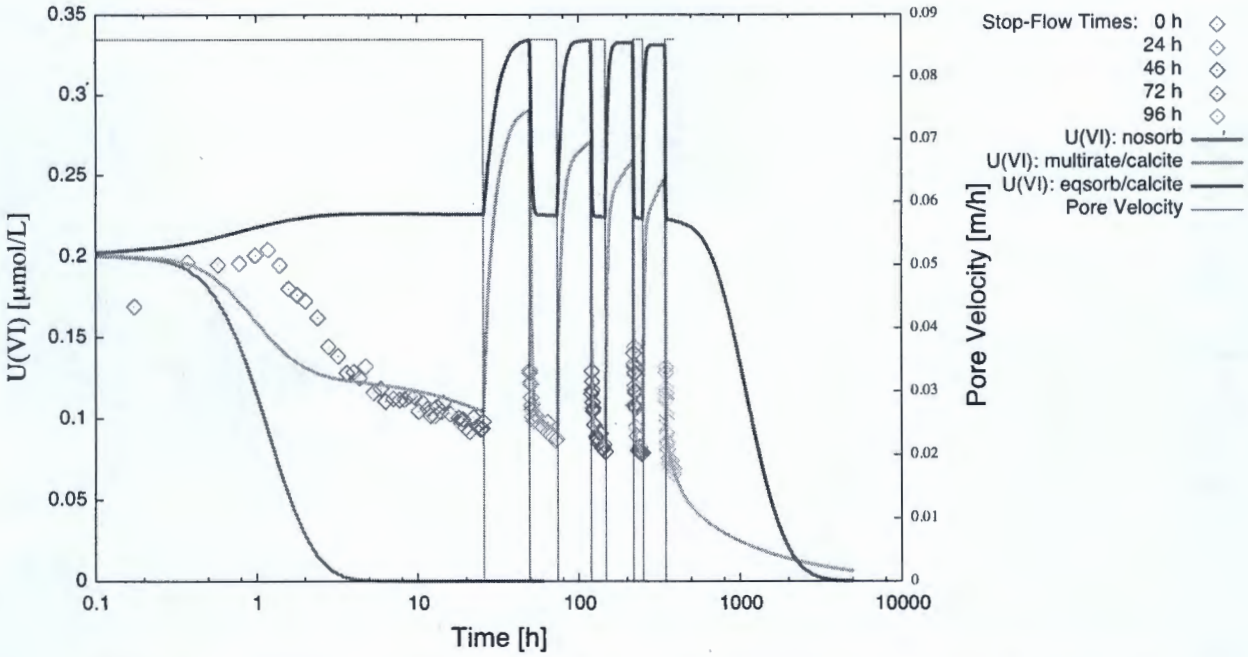

Figure 4. Comparison of breakthrough curves and internal U(VI) concentrations for the 1-D column experiment with calcite present, for the cases without sorption, and for equilibrium and multirate sorption models over long time spans. As can be seen from the figure, the multirate breakthrough curve is bracketed by the no sorption and equilibrium sorption cases except at very long times. The symbols refer to the small column experiment discussed by *Liu et al.* [2008].

from concentrated waste streams that presumably occurred during disposal. As a consequence of these considerations it is apparent that a first principles approach beginning with waste deposition is presently not, and may never be, feasible. Thus a more pragmatic approach must be implemented.

[37] One formulation of initial conditions is to begin the calculation without any U(VI) initially sorbed in the sediment outside the source region (i.e., between the source region and river). However, this approach would require long simulation times due to the relatively high retardation of U(VI) by the Hanford sediment under present-day conditions and does not conform to actual conditions of waste emplacement. Therefore, instead of attempting to calculate the current in-ground U(VI) distribution starting from pristine sediment conditions, in this study the initial time ($t = 0$) is set to correspond to the time when the U(VI) plume already extends from the source region to the river as currently observed. This requires specifying the initial solid phase deposition of U(VI) after waste emplacement has ceased. Evidence exists for the presence of two distinct forms of U(VI) in contaminated Hanford sediment [*McKinley et al.*, 2007; *Singer et al.*, 2009; *Stubbs et al.*, 2009; D. L. Stoliker et al., Characterization of metal-contaminated sediments: Distinguishing between samples with adsorbed and precipitated metal ions, submitted to *Environmental Science and Technology*, 2009]. One form is the more easily removed, exchangeable, labile fraction which consists primarily of sorbed U(VI) [*Bond et al.*, 2008]. As already noted, labile U(VI) stored in the vadose zone provides a source of U(VI) that is periodically released as the water table rises and falls as a result of fluctuations in the river stage. The other less readily dissolved nonlabile form occurs in mineralized and amorphous phases and may also be coprecipitated with calcite [*Bond et al.*, 2008; *Singer et al.*, 2009; *Stubbs et al.*, 2009; Stoliker et al., submitted manuscript, 2009]. Metatorbernite, for example, has been observed in small quantities in the NPP [*Catalano et al.*, 2006; *Arai et al.*, 2007; *Singer et al.*, 2009]. The findings of *Singer et al.* [2009] suggest that both dissolution of U(VI)-Cu(II)-bearing solids as well as U(VI) desorption are important persistent sources of U(VI). However, the exact form of nonlabile U(VI) still remains elusive to this day.

[38] In the presence of present-day dilute, oxidizing groundwater compositions it is reasonable to expect that bulk pore waters are undersaturated with respect to nonlabile forms of U(VI), with the possible exception of the vadose zone where complete or partial dry out could lead to higher U(VI) concentrations.

[39] In the evolution from initial waste emplacement to complete removal of U(VI), three distinct phases are identified roughly corresponding to three different periods in time:

[40] ***Phase I:*** Initial time period of U(VI) disposal and establishing the U(VI) plume with occupation of sorption sites between the source region and river.

[41] ***Phase II:*** Intermediate time period of continued removal of U(VI) from the source region with the U(VI) plume in place between the source region and the river.

[42] ***Phase III:*** Final time period following complete removal of nonlabile U(VI) from the source region and sorbed labile U(VI) from the vadose zone with U(VI) migration controlled by desorption and sorption processes.

[43] Of course, overlap exits between the different phases (time periods). Each phase has its unique set of initial conditions corresponding to $t = 0$. A transition period exists

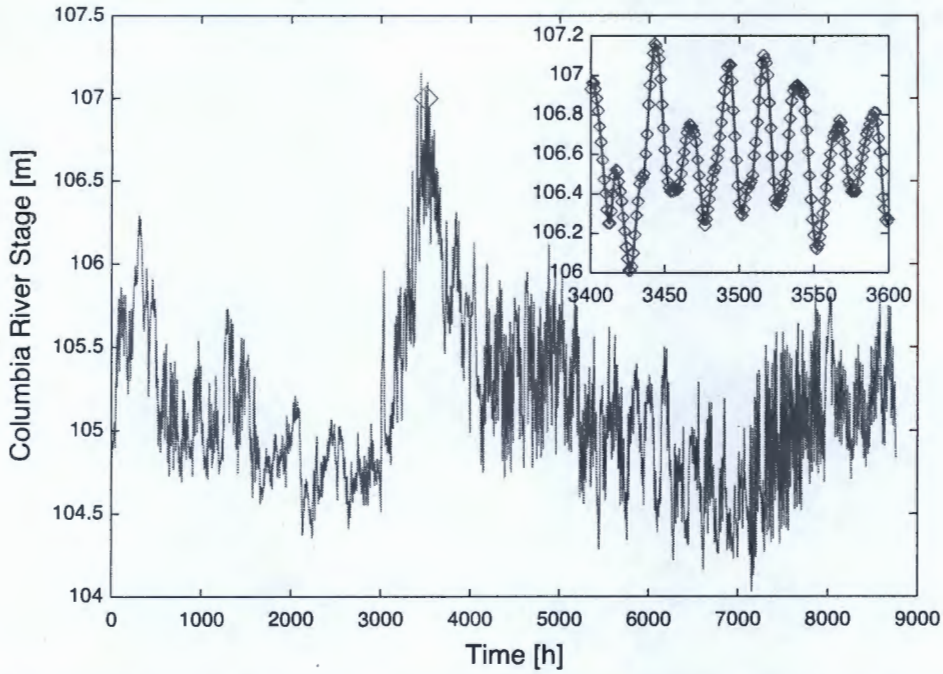

Figure 5. Fluctuations in the Columbia River stage illustrating daily, weekly, and seasonal variations. The symbols in the insert represent hourly time increments.

as the system evolves from Phase II to Phase III as the nonlabile U(VI) gradually disappears. This work is focused on modeling Phase II.

[44] Phase I is too uncertain to model because there is little or no historical information for the composition of the waste stream at the site and a high-resolution data set for the time history of the Columbia River stage and inland groundwater piezometric head does not exist during this period. Furthermore, the South Process Pond clogged during operation requiring creation of the North Process Pond, suggesting a highly concentrated waste form (J. M. Zachara, personal communication, 2009). Phase III is investigated briefly in 1-D scoping calculations, but reserved for the subject of a future 3-D modeling study, because of the longer time span required of at least tens of years, a computationally challenging effort due to the short time steps, on the order of hours, required to resolve river stage fluctuations.

[45] One difficulty with implementing initial conditions for Phases II and III, however, is that the detailed, in-ground distribution of U(VI) is not known with great accuracy, and furthermore, it changes continuously with time due to the rapidly fluctuating river stage. For the calculations reported in *DOE* [1994a, 1994b], an initial U(VI) plume was implemented based on observations from wells using the Phase III conceptual model. In this work, to set up approximate initial conditions for U(VI), the problem is first run without sorption, but with a nonlabile source term present with its rate adjusted to give the approximate maximum observed U(VI) concentration in the aquifer. This nonlabile source is provided in the form of a uranium-bearing mineral localized within the SPP several meters both above and below the mean position of the water table referred to as the smear zone. The mineral metatorbernite $[Cu(UO_2)_2\,(PO_4)_2 \cdot 8H_2O]$ is used for this purpose as a surrogate mineral.

[46] This initialization procedure allows a U(VI) plume to fully develop approximating present-day conditions in the region between the source and river. Following development of the plume, the sorption sites are equilibrated with the calculated spatial distribution of aqueous U(VI) based on the nonsorbing result. This procedure provides an approximate initial distribution of aqueous and sorbed concentrations of U(VI) along the flow path to the river corresponding to Phase II.

[47] For equilibrium surface complexation and multirate kinetic sorption, sorbed solute concentrations are equilibrated with aqueous solute concentrations from the stored initial condition for each control volume. To compute the sorption site concentration for bulk sediment, note that the <2 mm size fraction, the dominant location of sorption sites [*Liu et al.*, 2008; *Zachara et al.*, 2005], occupies approximately 10% by volume of the sediment. The bulk site density $\omega_\sigma^{\text{bulk}}$ is obtained from the fine-grained site density $\omega_\sigma^{\text{fine}}$ using the relation

$$\begin{aligned}\omega_\sigma^{\text{bulk}} &= \frac{N_s}{V} = \frac{V_{\text{fine}}}{V}\frac{N_s}{V_{\text{fine}}}, \\ &= \epsilon_{\text{fine}}\omega_\sigma^{\text{fine}},\end{aligned} \tag{43}$$

giving a value of $\omega_\sigma^{\text{bulk}} = 15.264$ mol/m^3 for $\epsilon_{\text{fine}} \simeq 0.1$.

4.3. 1-D Phase II and III Scoping Calculations

[48] To investigate the effects of fluctuating flow directions and sorption on the breakthrough of U(VI), several simple 1-D scoping calculations are performed for Phase II and III. These calculations are not meant to be realistic representations of the 300 Area, but merely serve to investigate the role of river stage fluctuations and the nonlabile leach rate on the U(VI) flux at the river boundary. The U(VI)

Table 3. Columbia River Solution Composition[a]

Species	Molality	Total	Activity Coeffficient	Constraint
H+	1.6604E-08	2.8937E-05	9.5452E-01	pH
Ca^{2+}	4.4070E-04	4.5078E-04	8.2334E-01	total
Cu^{2+}	3.7688E-10	1.0028E-08	8.2334E-01	total
Mg^{2+}	1.7796E-04	1.8284E-04	8.2758E-01	total
$UO2^{2+}$	5.0558E-18	2.4901E-11	8.2001E-01	total
K^+	1.9098E-05	1.9108E-05	9.5073E-01	total
Na^+	5.1296E-05	5.1392E-05	9.5141E-01	chrg
HCO_3^-	1.0823E-03	1.1311E-03	9.5141E-01	total
Cl^-	3.3985E-05	3.3992E-05	9.5073E-01	total
F^-	6.2190E-06	6.2504E-06	9.5107E-01	total
HPO_4^{2-}	6.5862E-10	1.0028E-09	8.1888E-01	total
NO_3^-	1.0010E-05	1.0028E-05	9.5073E-01	total
SO_4^{2-}	8.6604E-05	9.2657E-05	8.1888E-01	total

[a]Ionic strength, 2.0229E-03 (mol/L); Ph, 7.80; charge balance, 1.8974E-19; pressure, 1.0133E+05 (Pa); temperature, 25.00 (°C); density H_2O, 997.16 (kg/m^3).

Table 5. U(VI) Source Region Solution Composition[a]

Species	Molality	Total	Activity Coeffficient	Constraint
H+	5.4582E-08	2.1710E-04	9.1823E-01	pH
Ca^{2+}	2.4745E-03	2.6126E-03	6.9039E-01	calcite
Cu^{2+}	1.6478E-07	2.3101E-06	6.9039E-01	tenorite
Mg^{2+}	1.5909E-04	1.7293E-04	7.0315E-01	dolomite
UO_2^{2+}	2.5604E-15	2.3494E-07	6.8010E-01	total
K^+	1.5436E-04	1.5485E-04	9.0499E-01	total
Na^+	1.0296E-03	1.0354E-03	9.0748E-01	total
HCO_3^-	2.2818E-03	2.5741E-03	9.0748E-01	total
Cl^-	6.9734E-04	6.9803E-04	9.0499E-01	total
F^-	2.0725E-05	2.0958E-05	9.0625E-01	total
HPO_4^{2-}	1.0565E-06	2.4810E-06	6.7652E-01	hydroxylapatite
NO_3^-	4.6596E-04	4.7018E-04	9.0499E-01	total
SO_4^{2-}	5.4331E-04	6.3823E-04	6.7652E-01	total

[a]Ionic strength, 8.7143E-03 (mol/L); pH, 7.30; charge balance, 1.9334E-03; pressure, 1.0132E+05 (Pa); temperature, 25.00 (°C); density H_2O, 997.16 (kg/m^3).

flux for both equilibrium and multirate surface complexation are compared for different metatorbernite rate constants. A computational domain of 500 m is used in the simulations. The pressure at the inland boundary is fixed to give a mean flow rate to the river of 1 km/yr. The pressure at the outlet is allowed to fluctuate using the same river stage height shown in Figure 5. For Phase II a source region 50 m wide containing metatorbernite is placed at a distance of 250 m from the outlet. For both Phase II and Phase III, sorption sites in the region between the source and the outlet are equilibrated with U(VI).

[49] A total of 13 primary species {H^+, Ca^{2+}, Cu^{2+}, Mg^{2+}, UO_2^{2+}, K^+, Na^+, HCO_3^-, Cl^-, F^-, HPO_4^{2-}, NO_3^-, SO_4^{2-}} are used in the simulations in addition to two tracers for a total of 15 degrees of freedom. Eighty-eight secondary aqueous complexes, two minerals (calcite and metatorbernite), and two surface complexes are also used. For geochemical transport, chemical compositions with the exception of Cu^{2+} and HPO_4^{2-} for background river water (Table 3) and groundwater (Table 4) were obtained from J. P. McKinley (personal communication, 2009) and USGS data (Water data reports for the Columbia River at Vernita Bridge, near Priest Rapids Dam, Washington, for site 1247900, 2001–2007, http://pubs.usgs.gov/wdr), respectively, and assigned to the western inland and river seepage face boundaries, respectively. The river water has a slightly higher pH compared to groundwater, but lower carbonate concentration. A representative fluid composition for the spatially variable distributed source region is listed in Table 5.

Table 4. Hanford Sediment Groundwater Solution Composition[a]

Species	Molality	Total	Activity Coeffficient	Constraint
H^+	2.7478E-08	1.0949E-04	9.2508E-01	calcite
Ca^{2+}	1.1376E-03	1.2099E-03	7.1492E-01	total
Cu^{2+}	3.4392E-10	1.0028E-08	7.1492E-01	total
Mg^{2+}	4.6636E-04	5.1122E-04	7.2578E-01	total
UO_2^{2+}	6.3727E-19	2.4901E-11	7.0620E-01	total
K^+	1.5477E-04	1.5523E-04	9.1414E-01	total
Na^+	1.3376E-03	1.3451E-03	9.1618E-01	chrg
HCO_3^-	2.4079E-03	2.5804E-03	9.1618E-01	total
Cl^-	6.9934E-04	6.9973E-04	9.1414E-01	total
F^-	2.0768E-05	2.1009E-05	9.1517E-01	total
HPO_4^{2-}	8.9133E-10	1.6774E-09	7.0318E-01	fluorapatite
NO_3^-	4.6938E-04	4.7132E-04	9.1414E-01	total
SO_4^{2-}	5.6010E-04	6.3978E-04	7.0318E-01	total

[a]Ionic strength, 6.9033E-03 (mol/L); pH, 7.59; charge balance, −2.1684E-19; pressure, 1.0133E+05 (Pa); temperature, 25.00 (°C); density H_2O, 997.16 (kg/m^3).

[50] Shown in Figure 6 are 1-D results for the cumulative flux of U(VI) at the outlet boundary. According to the figure, an essentially constant slope in the cumulative U(VI) flux is obtained, in spite of the rapid oscillatory behavior of the Columbia River stage. A change in slope occurs at approximately 4 years for the cases for an effective metatorbernite rate constant of 5×10^{-17} and 10^{-16} mol/cm^3/s (red and blue curves), indicating that U(VI) released from dissolution of metatorbernite has reached the river boundary. The case for an effective rate constant of 7×10^{-17} mol/cm^3/s shows no noticeable change in slope. The rate law given in equation (18) without the prefactor $\mathcal{P}_m$ is used in the simulations.

[51] A change in slope implies that the initial distribution of sorbed U(VI) between the source region and the river, and the effective dissolution rate of the nonlabile U(VI) source, may not necessarily be consistent with one another. This average flux will in general be different for the release of U(VI) from the initially sorbed sediment and from the U(VI) released through mineral dissolution from the source region. As it takes several years for U(VI) released from the source region to reach the river, one would expect to observe a change in slope in the cumulative U(VI) flux when this U(VI) reaches the river. This new slope corresponds to the combined effect of U(VI) released from the source region at a specified rate and sorption reactions with U(VI)-bearing surface sediment sites, and should reflect present-day conditions more accurately than the originally specified initial conditions. Ideally, these conditions should be used for the initial conditions and time $t = 0$ set to the onset of the new slope in the cumulative flux. One may note that multirate sorption has a slightly lower slope compared to equilibrium sorption for the same metatorbernite rate constant of 7×10^{-17} mol/cm^3/s. This is presumably a consequence of a slightly lower U(VI) concentration in the multirate case which also affects the dissolution rate through the rate affinity factor.

[52] As can be seen from Figure 6, for Phase III with metatorbernite absent and only sorbed U(VI) present ini-

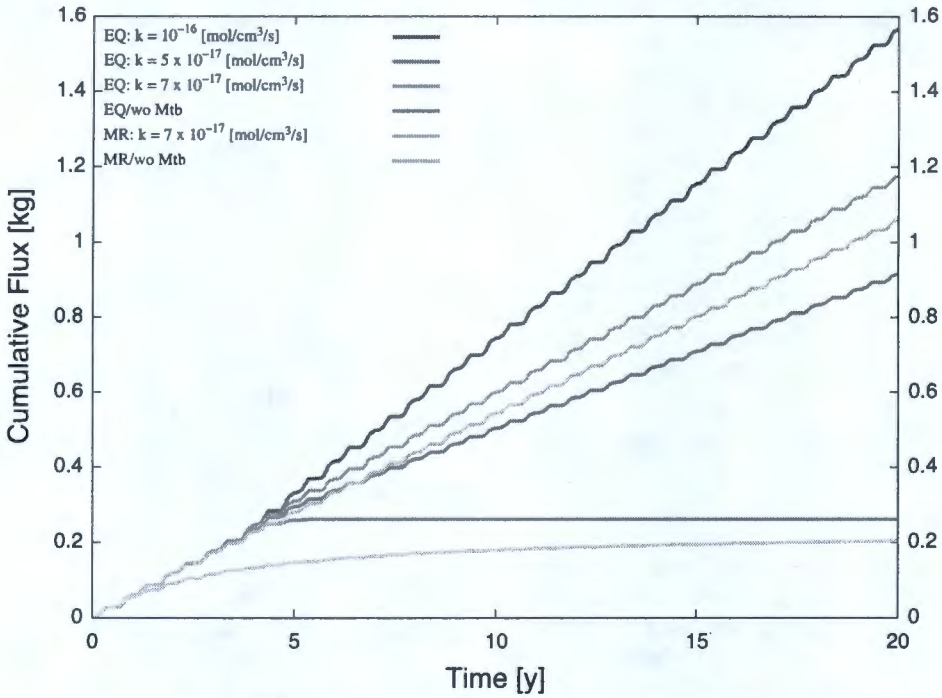

Figure 6. Comparison of the cumulative U(VI) flux for different source-term production rates for Phase II initial conditions and equilibrium and multirate sorption models for Phase III conditions.

tially, all U(VI) is removed in approximately 5 years for the equilibrium model, with a more gradual release for the multirate sorption model which requires approximately 20 years to remove all U(VI). According to Figure 6, the multirate model does not give a significantly different result compared to the equilibrium sorption model for Phase II, but gives very different results for Phase III initial conditions requiring a much longer time for U(VI) to become depleted from the source region compared to the equilibrium model. In contrast to a 1-D model, in a 3-D model not all of the nonlabile U(VI) will disappear uniformly, rather one might expect a more gradual decrease accompanied by a reduction in the reacting surface area with time.

5. 3-D Simulations of the Hanford 300 Area Uranium Plume

[53] In this section 3-D simulations are carried out to model natural attenuation of U(VI) at the Hanford 300 Area using high-performance computing with PFLOTRAN [*Hammond et al.*, 2008]. The calculations employ a high-resolution, variably saturated domain with over 28 million degrees of freedom including 15 chemical components. High performance computing is required for the calculations because of the large 3-D problem size and small time steps. For a 1 year simulation with 4096 processor cores, PFLOTRAN requires a computation time of approximately 6 h due to the 1 h time step limitation dictated by the need to capture river stage fluctuations in the simulations. With 4096 processor cores, roughly the optimal number of cores for this problem for solving the reactive transport equations, there are 6855 dof/core for transport and a factor of 15 less for flow. If this problem could be run on a comparable single processor workstation, assuming no memory limitation, it would require nearly 3 years of cpu time. The 3-D calculations were carried out on ORNL's Jaguar supercomputer. The Jaguar XT4 partition has a total of 7,832 compute nodes or 31,328 cores, with an aggregate system performance of approximately 263 teraflop/s at the time of this writing. The machine is continuously being upgraded to the latest chipsets available. The Jaguar XT5 partition has a total of 18,688 nodes or 224,256 cores, with a peak performance of 2.33 petaflop/s. The interested reader can visit the Web page http://www.nccs.gov/jaguar/ for the most up-to-date configuration of the machine.

[54] The simulations may be compared against three observations at the site: (1) field data for the piezometric head at various wells; (2) estimated U(VI) and water fluxes at the river-aquifer boundary based on field experiments [*Fritz et al.*, 2007; *Fritz and Arntzen*, 2007; *Peterson et al.*, 2009]; and (3) the maximum observed aqueous U(VI) concentrations. Comparison with observed time histories of U(VI) concentrations is not possible because of the lack of data for the time period used in setting the inland piezometric head boundary conditions. By contrast, the model has only two adjustable parameters, namely, the conductance boundary condition imposed at the river-aquifer interface and the U(VI) source-term rate, and thus is overdetermined. Presumably in the future, the source-term rate could be directly measured and used as input to the model and thereby test the consistency of the model results. The current model domain includes the footprint of the SPP as the source region for nonlabile U(VI). In the future, the NPP, trenches and an extended smear zone [*Williams et al.*, 2007] will also need to be included in the simulation.

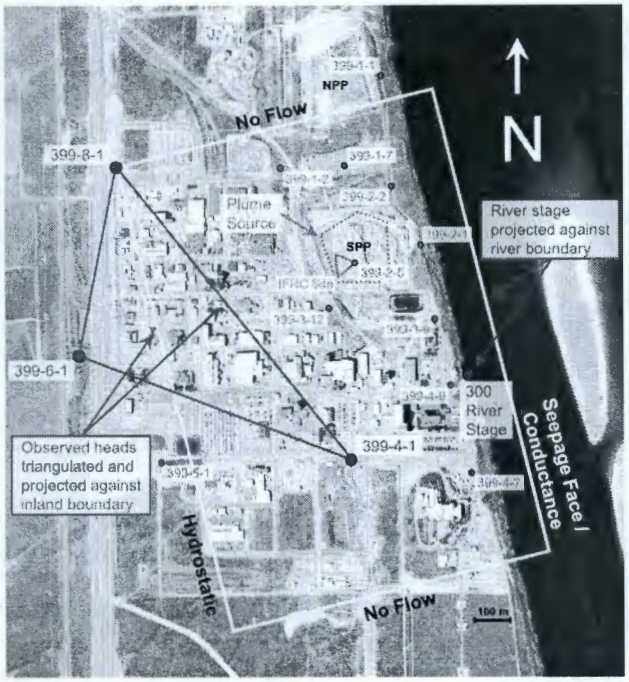

Figure 7. Planar view of outline of 3-D computational domain (yellow line) showing the locations of the North and South Process Ponds (NPP and SPP), the IFRC field site, and a subset of observation wells. The transient inland boundary condition at the western edge is constructed by projecting head data obtained from wells 399-8-1, 399-6-1, and 399-4-1 onto the western boundary. The transient Columbia River stage is projected onto the river boundary to the east. No-flow boundary conditions are imposed on the north and south faces.

5.1. Computational Domain

[55] The model of the Hanford 300 Area used in this work consists of a problem domain measuring 900 × 1300 × 20 meters (x, y, z) with orientation aligned with the Columbia River at 14° west of north (Figure 7). The base of the model domain lies at an elevation of 90 meters above sea level. Simulations were performed on a Cartesian grid with spacing 5 meter horizontal × 0.5 meter vertical with 180 × 260 × 40 = 1,872,000 grid cells. Thus total number of flow degrees of freedom (unknowns) is equal to 1,872,000 with 1 dof/cell, while the number of degrees of freedom for the geochemical transport equations is 28,080,000 with 15 chemical components (15 dof/cell).

[56] The Hanford and Ringold geologic units are mapped to the prescribed grids based on the Hanford EarthVision database [*Thorne et al.*, 2006; *Williams et al.*, 2008; *Bjornstad et al.*, 2009]. The soils beneath the Hanford 300 Area are composed of layers of high- and low-permeability soil, the top layer of which is the highly permeable Hanford Unit extending from the vadose zone down into the saturated zone below the water table. The Hanford Unit is composed of highly permeable cobbles, gravels, and sands. Hydraulic conductivities (K) within the Hanford Unit are on the order of a thousand to tens of thousands of meters per day ($k = 10^{-9} - 10^{-8}$ m^2). In comparison, the Ringold Units below the Hanford Unit exhibit much lower hydraulic conductivities of 0.01 to 150 meters per day ($k = 10^{-14} - 1.58 \times 10^{-10}$ m^2). Thus, within the Hanford Unit groundwater has the potential of flowing rapidly with very small pressure gradients in the aquifer. Values for permeability used in the simulations for the Hanford Unit are 7.387×10^{-9} m^2 (K = ~7000 m/day) in the x and y directions and a factor of 10 lower in the z direction, with a porosity of 0.2 [*Williams et al.*, 2008, Table 3.4: r5b-b]. These values were obtained from manual calibration to slug tests (M. Rockhold, personal communication, 2009). A combination of van Genuchten and Burdine capillary functions are used with $\alpha = 7.2727 \times 10^{-4}$ Pa^{-1}, $\lambda = 0.3391$ and $s_r = 0.16$.

5.2. Initial and Boundary Conditions and Nonlabile Source

[57] To set up initial conditions corresponding to Phase II, it is necessary to determine the initial distribution of sorbed U(VI) as well as the initial solution composition. As described in section 4.2, initial conditions are set by running a non-sorbing simulation for several years, at which time a uranium plume is well established and intercepts the river boundary. At that time, the 3-D aqueous concentration profile is frozen and used as the initial condition for subsequent simulations. The total inventory of U(VI) contained in both the aqueous and sorbed phases is 1,974 kg which is consistent with the mass balance estimate of *Peterson et al.* [2009] of several thousand kilograms. It is unknown how much the nonlabile form of U(VI) contributes to the total in-ground inventory.

[58] Determining the precise boundary conditions to impose on the 3-D domain is complicated by the lack of well data in the vicinity of the inland boundary and the complex hydrology at the site caused by the fluctuating river stage. The northern, southern, and bottom boundaries of the domain are prescribed as no flow conditions. This is clearly an approximation, but is considered reasonable because groundwater converges at the Hanford 300 Area from the northwest, west, and southwest [*Peterson et al.*, 2005], and the site exhibits a relatively flat gradient toward the river. Transient flow boundary conditions are used at the river boundary and inland at the west face of the domain to account for the highly oscillatory fluctuations in the Columbia River stage. A seepage face or conductance boundary condition is imposed at the river boundary. The pressure gradient along the river is calculated from the piezometric head at wells 399-1-1, 399-2-1 and 399-4-7 that are close to the river. The seepage face boundary condition is essentially a hydrostatic condition with minimum boundary pressures truncated at atmospheric pressure. A transient hydrostatic pressure boundary condition is imposed at the western inland boundary. This boundary condition is determined through projection of piezometric heads at nearby wells 399-8-1, 399-6-1, and 399-4-1 onto the western domain boundary. At these wells, a year of data is available between 8 pm December 25, 1992 and 8 pm December 25, 1993. These data in conjunction with river stage and gradient from the same time period are employed and cycled yearly in the transient boundary conditions.

[59] Aside from the initial distribution of U(VI) in the problem domain (i.e., the initial U(VI) plume), the model contains only two parameters that are not directly deter-

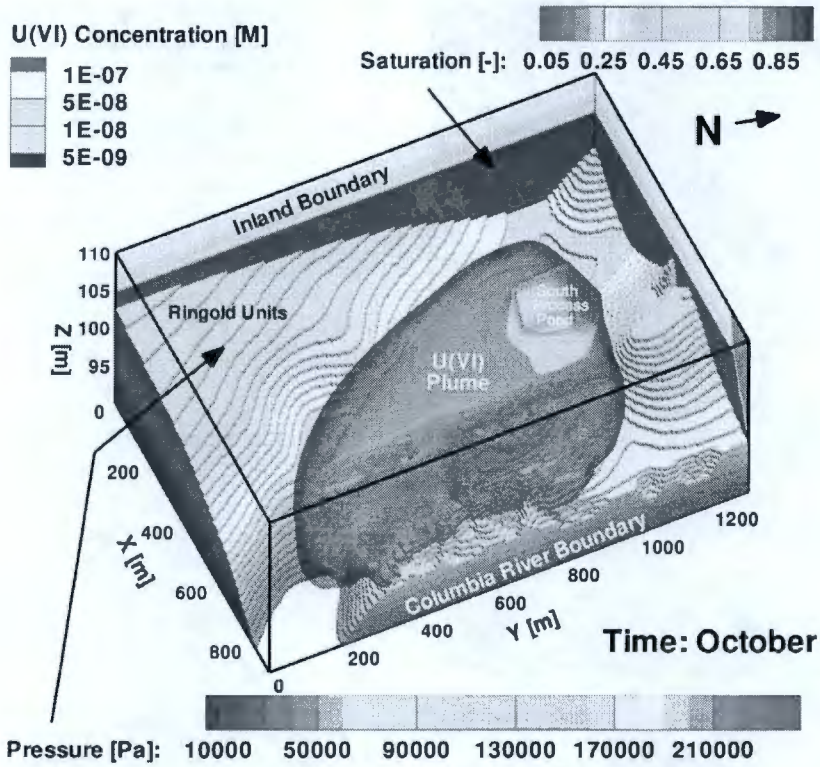

Figure 8. Three-dimensional isosurfaces for the concentration field of the U(VI) plume, saturation (side panels), and pressure draped on the contact between the Hanford (hidden) and Ringold formations. The Columbia River and inland boundaries are also indicated. The U(VI) source region is located at the South Process Pond. The domain size measures 900 m × 1300 m × 20 m.

mined by field or laboratory data; namely, the value for the conductance coefficient at the river-aquifer interface representing the hyporheic zone and the effective rate constant for the nonlabile source term. All other parameters are constrained through site-specific data including material properties such as permeability and porosity, and sorption properties of the sediment. The conductance coefficient at the river-aquifer boundary is determined by comparing model results to the observed head at well 399-2-1 located along the river just east of the Hanford 300 Area South Process Pond and Integrated Field Research Challenge (IFRC) site (see Figure 7).

[60] A distributed initial source for U(VI) is implemented using metatorbernite as a surrogate mineral for Phase II. The metatorbernite effective kinetic rate constant is adjusted to give approximately the maximum concentration of U(VI) observed at the site using a value of 2×10^{-17} mol/cm^3/s. A value for the metatobernite equilibrium constant of $\log K = -31$ was chosen so that it remained undersaturated below the water table, but could reach equilibrium or even precipitate above the water table within the smear zone as a result of dry out. More recently *Ilton et al.* [2010] have obtained a value of $\log K = -28$ for metatorbernite. This lower value will lead to greater undersaturation and would require using a lower metatorbernite rate constant so as not to exceed the maximum observed U(VI) aqueous concentration. Other U (VI)-bearing minerals such as uranyl-silicate minerals could also have been used in the simulations. As a consequence of fluctuations in the water table, sources of uranium residing immediately above the water table in the vadose zone are cyclically flushed over time as the water table rises and falls, releasing uranium into the underlying aquifer. Therefore, a quantitative description of the groundwater flow processes beneath the Hanford 300 Area is critical for capturing such behavior in the uranium transport model.

[61] Generally it would be expected that the multirate kinetic rate constants should be scaled just like any other effective parameter in a continuum model when applying rate constants derived from the column scale to the field scale. However, because it is unclear how the rate constants should be scaled, in what follows the same rate constants fit to the 1-D small column experiment by *Liu et al.* [2008] are used at the field scale. As is demonstrated below sorption plays only a secondary role for Phase II in determining the flux of U(VI) into the river, and therefore the results obtained are not significantly affected by the choice of rate constants in the multirate model.

5.3. Model Results

[62] Model results are presented for Phase II with both labile and nonlabile forms of U(VI) initially present. Reaction of the nonlabile U(VI) form is simulated by the dissolution of the surrogate mineral metatorbernite with an effective kinetic rate constant chosen to reproduce the maximum U(VI) concentration observed in the source region near well 399-2-5 [*Hartman et al.*, 2007].

Table 6. Description of Model Simulations and Predicted U(VI) Fluxes in kg/yr Calculated by Fitting the Cumulative Flux to a Linear Function of Time[a]

Run	Run Description	Conductance C (m)	Predicted U(VI) Flux (kg/yr)
1	equilibrium sorption	10^{-12}	25.47
2	no sorption	10^{-12}	25.67
3	multirate model	10^{-12}	25.80
4	equilibrium sorption	10^{-11}	45.16
5	equilibrium sorption	10^{-13}	5.81
6	equilibrium sorption	(seepage face)	64.72

[a]Run 1 is the baseline case with a conductance coefficient of 10^{-12} m, which is adjusted to better match the measured piezometric head at well 399-2-1.

[63] Six runs are carried out to test the sensitivity of the predicted flux of U(VI) into the Columbia River with the model parameters listed in Table 6. Runs are compared for the cases with no sorption, equilibrium and multirate sorption, and for different river boundary conductance coefficients with $C = 10^{-11}$, 10^{-12} and 10^{-13} m, and a seepage face (i.e., no conductance boundary condition). U(VI) concentration, saturation and pressure in the October time frame are depicted in Figure 8 for Run 1, which is taken as the base case.

5.3.1. Model Comparison With Measured Piezometric Head

[64] The conductance coefficient is determined by comparing the piezometric head predicted by the model with observation. This parameter together with the permeability of the Hanford Unit controls the flow velocity throughout the modeled aquifer and thus the U(VI) flux to the river. According to *Fritz and Arntzen* [2007], the permeability at the river-aquifer interface is highly heterogeneous with a wide range of values from 6.65×10^{-13} to 1.09×10^{-10} m^2 at their study area. A comparison of the simulated and measured piezometric head at well 399-2-1 is shown for different conductance coefficients in Figure 9 and in Figure 10 over smaller time intervals. As can be seen from the figures, the predicted head is highly sensitive to the choice of conductance coefficient. Reasonable agreement with observation is obtained for Run 1 using a conductance coefficient of 10^{-12} m. Without accounting for the reduced permeability at the river boundary through the conductance boundary condition, the head overshoots the observed values by a considerable amount as shown in the figures. This overshooting underscores the importance of the hyporheic zone on the flow rate and predicted movement of uranium in the subsurface at the 300 Area.

[65] The Darcy flow velocity at the location of well 399-2-5 is shown in Figure 11 as a function of time. The x, y, and z velocities show a complex behavior with time changing in direction and magnitude with hourly fluctuations. Flow cycles back and forth with large fluctuations predominantly in the x direction, with a significant component in the southerly y direction resulting in a mean flow to the southeast. At the location of well 399-2-1, located closer to the river, a similar pattern is obtained but with higher fluctuations. The calculated mean velocity toward the river $\overline{q}_x$ for wells 2-5 and 2-1 is 67.7 and 79.3 m/yr, respectively. The z velocity is smaller due in part to the lower permeability in the z direction and smaller vertical pressure gradient.

[66] To see the effect of the flow field on the solution composition, shown in Figure 12 is the total aqueous U(VI) and carbonate concentrations and pH at well 399-2-1 at an elevation of 104 m. As river water intrudes from 0.35 to 0.4 years, the pH sharply rises and the U(VI) and carbonate concentrations decrease. Then, as flow is reversed and river water begins to recede, the U(VI) and carbonate concentra-

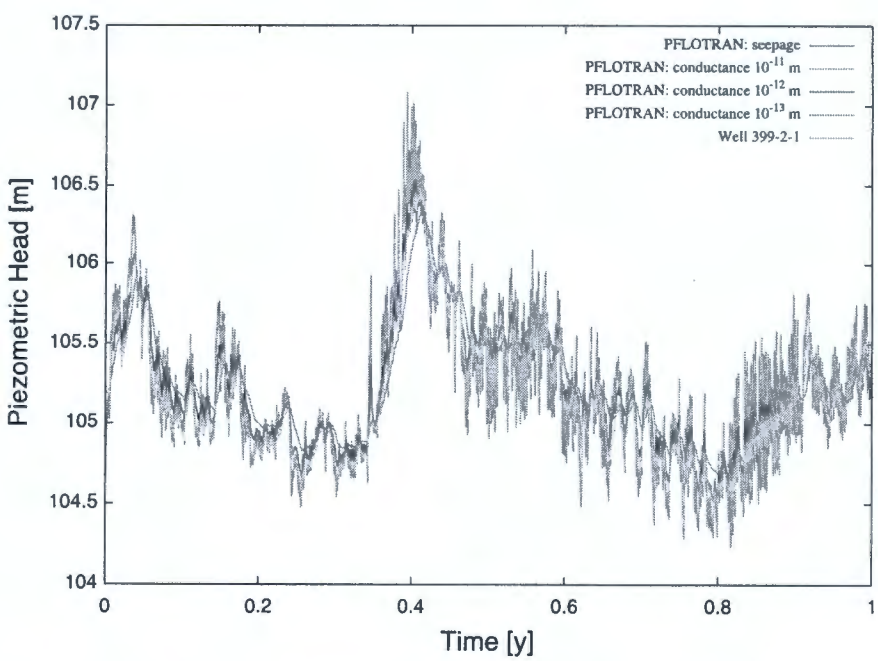

Figure 9. Comparison of the observed piezometric head at well 399-2-1 with PFLOTRAN for a seepage river boundary condition and different conductance coefficients. Of the four cases considered, a conductance coefficient of 10^{-12} m gives the better match to the data.

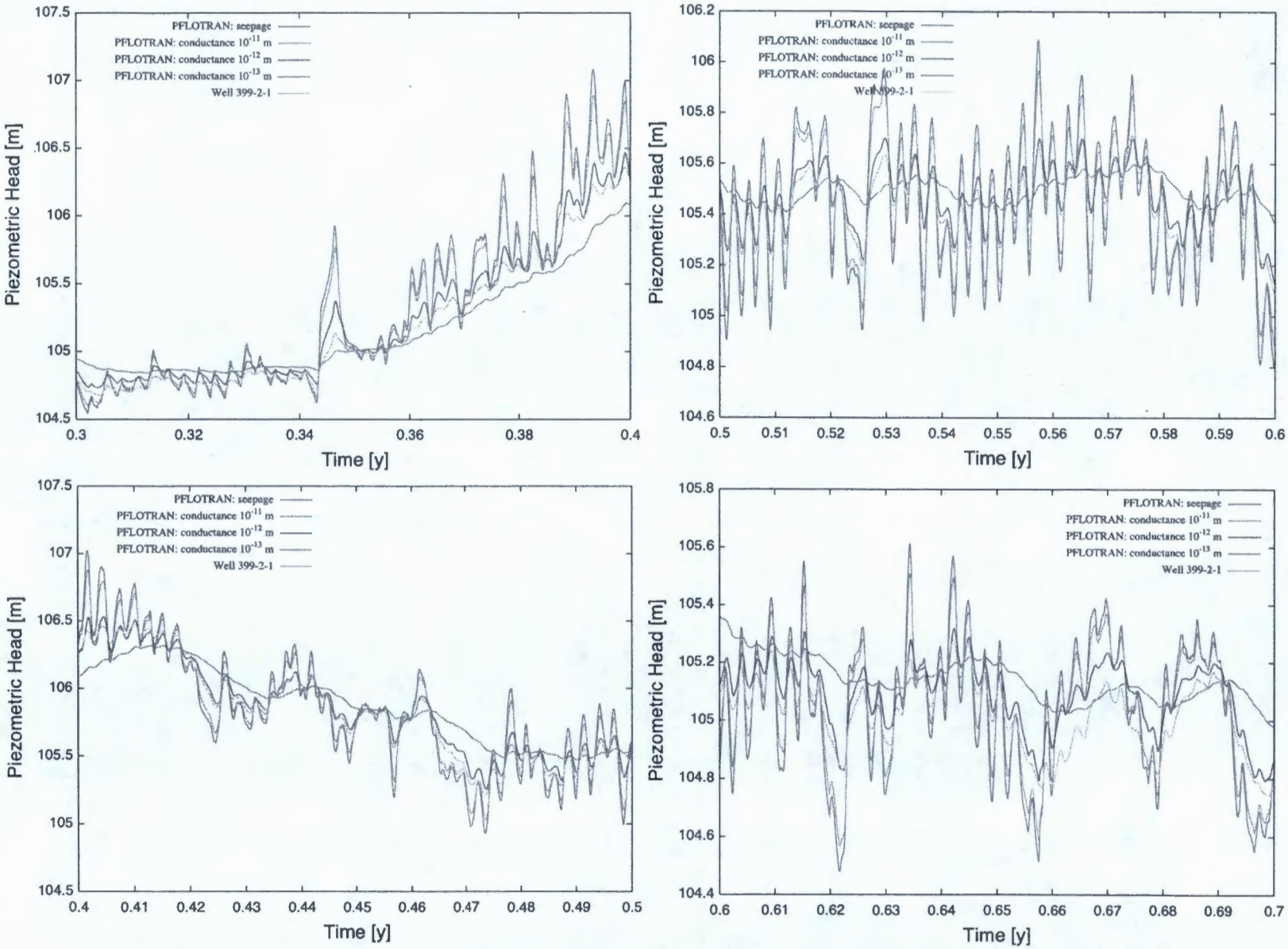

Figure 10. Magnification of Figure 9 for smaller time intervals comparing the piezometric head at well 399-2-1 with PFLOTRAN for a seepage river boundary condition and different conductance coefficients.

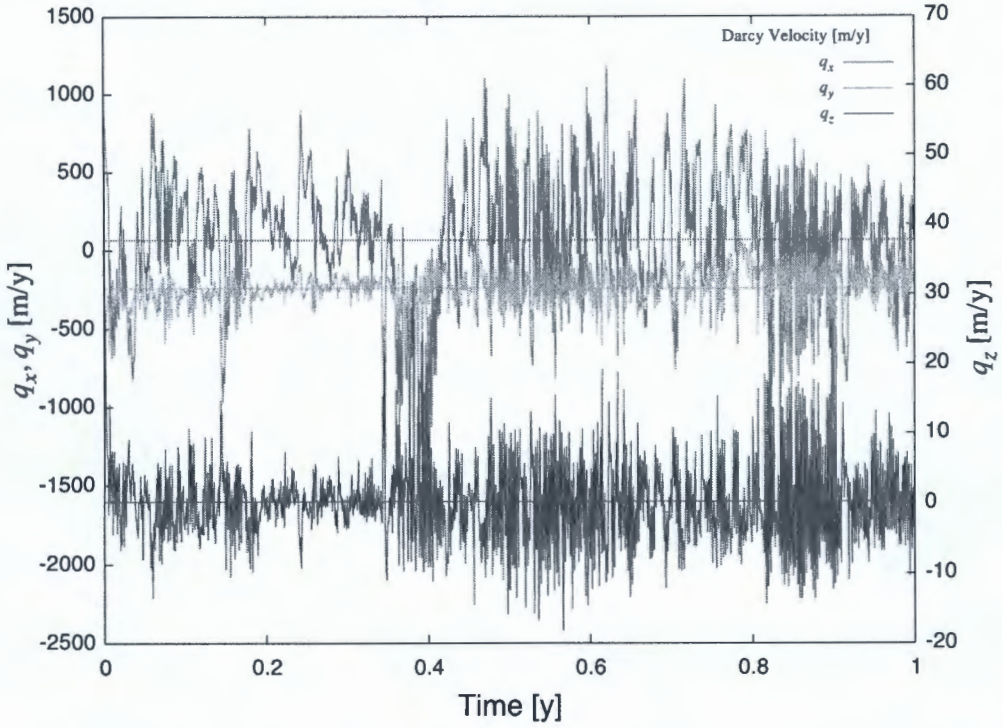

Figure 11. Fluctuation in the Darcy flow velocities q_x, q_y, and q_z calculated at the position of well 399-2-5 at an elevation of 104 m with mean values 67.26, −241.45, and 0.225 m/yr, respectively, for a conductance coefficient of 10^{-12} m.

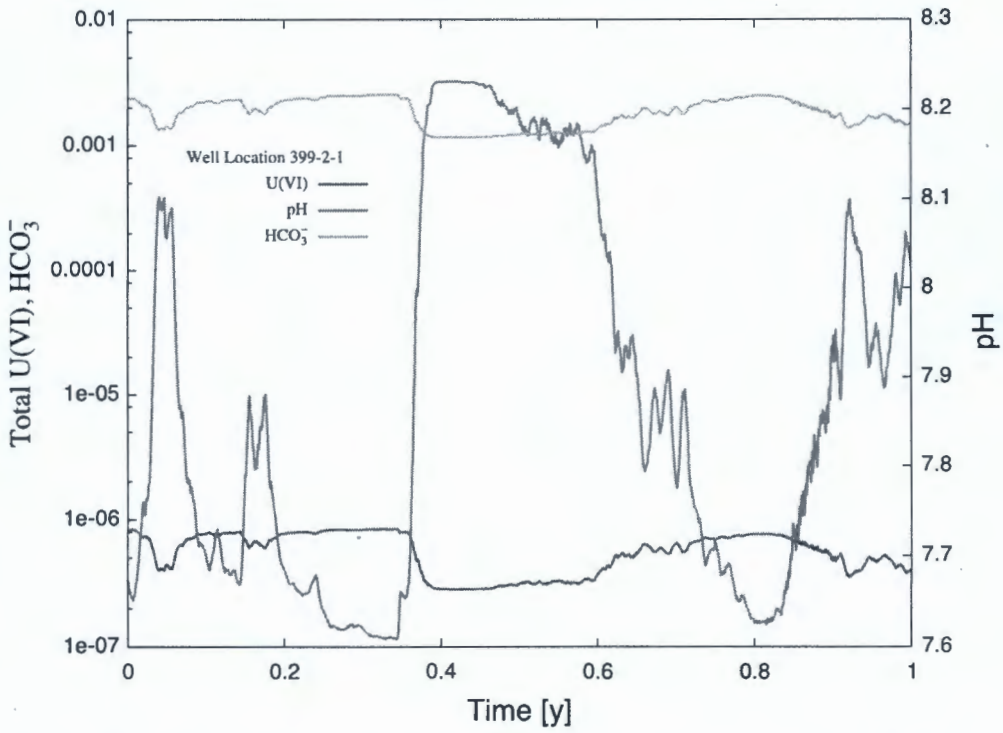

Figure 12. Plot of the total aqueous U(VI) and carbonate concentrations (mol/L) and pH as a function of time for a conductance coefficient of 10^{-12} m at the location of well 399-2-1 at an elevation of 104 m.

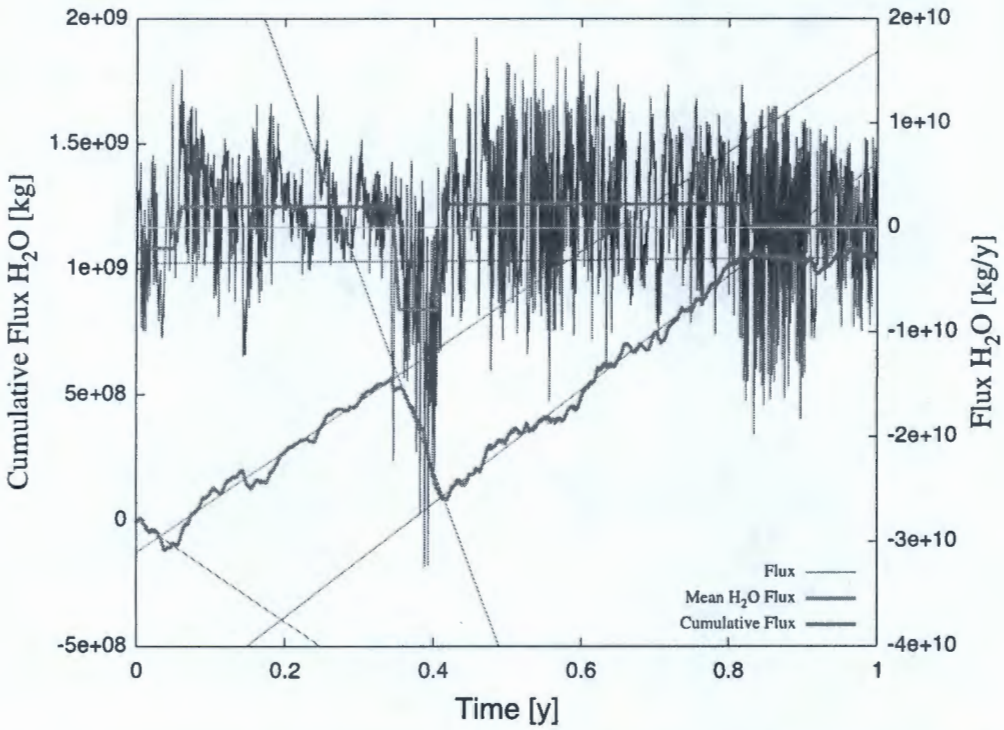

Figure 13. Instantaneous and cumulative water flux at the river-aquifer boundary plotted as a function of time for a conductance coefficient of 10^{-12} m. The mean flux given by the step function (purple line) is equal to the slope of the linear fits to the cumulative flux as indicated by the thin straight red lines.

tions gradually increase and the pH decreases. The concentrations do not show the rapid oscillatory behavior typical of the flux as discussed next.

5.3.2. H_2O and U(VI) Flux Estimates

[67] The cumulative and instantaneous flux for the base case Run 1 for H_2O is shown in Figure 13. Shown in Figure 13 are fits to the cumulative flux with lines of constant slope between flow reversals. The mean values obtained from the fit are listed in Table 7 along with an estimated mean flow velocity. Surprising is the emergence of lines of constant slope resulting from time averaging the instantaneous H_2O flux. Flow toward the river generally occurs over longer periods of time compared to the reverse direction for this time period. The time integral of the flux F averaged over the river boundary yields to a good approximation a linear increase with time according to the result

$$\mathcal{F}(t) = \int_{t_0}^{t} dt' F(t') \simeq \overline{F} \cdot (t - t_0), \tag{44}$$

where $\overline{F}$ denotes the mean flux. This result is a consequence of the approximation that variations in the flux about the mean $\delta F = F - \overline{F}$ average to zero over a time interval Δt that is small compared to macroscopic changes in the flux, but large compared to hourly fluctuations; thus

$$\int_{\Delta t} dt \delta F(t) \simeq 0. \tag{45}$$

The average H_2O flux of approximately 10^9 kg/yr agrees well with previous estimates [*Williams et al.*, 2008]. Figure 14 compares the effect of conductance and the seepage boundary condition on the cumulative H_2O flux to the river. A lower conductance coefficient leads to a decrease in the cumulative flux.

[68] The instantaneous and cumulative fluxes at the river-aquifer boundary for U(VI) are shown in Figure 15a, while the ratcheting effect of the release of U(VI) into the Columbia River when the flux is positive is illustrated in Figure 15b. The mean values for the U(VI) flux are listed in Table 6 for the six different cases considered. The instantaneous U(VI) flux exhibits a highly oscillatory behavior. However, as can be seen from Figure 15, the cumulative flux varies approximately linearly in time over the entire time interval in distinct contrast to H_2O which exhibits a zigzag behavior as flow changes direction to and from the river. The slope of the straight line fit to the cumulative flux is 24.76 kg/yr which compares favorably with the estimated value of 20–50 kg/yr by *Peterson et al.* [2009]. Very little difference in the cumulative flux is found between the

Table 7. Flux for H_2O in kg/yr for the Base Case Run 1 With a Conductance Coefficient of 10^{-12} m Calculated by Fitting the Indicated Time Intervals to a Linear Function of Time

	H_2O Flux for Run 5	
Time Interval (year)	Flux (kg/yr)	Darcy Velocity[a] (m/yr)
0.00–0.06	-2.02×10^9	−77.84
0.06–0.35	2.00×10^9	77.08
0.35–0.41	-7.87×10^9	−303.30
0.41–0.82	2.26×10^9	87.10
0.82–1.00	-2.30×10^7	−0.89

[a]The velocity is based on the geometric conductance boundary surface area of 20×1300 m^2 at the river-aquifer interface.

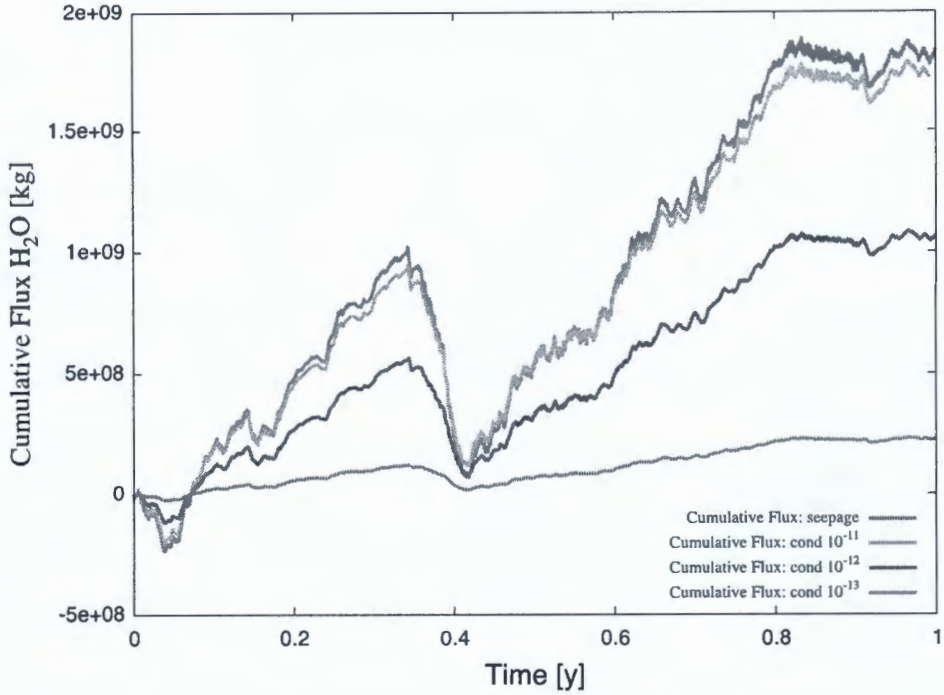

Figure 14. Cumulative water flux for different conductance coefficients at the river boundary. The value 10^{-12} m gives the best fit to the observed head at well 399-2-1.

equilibrium and the multirate sorption models. This may be due to the fact that the sorbed U(VI) is initially equilibrated with the aqueous phase, however this result is surprising considering the dramatic fluctuations in aqueous U(VI) concentration that occur throughout major portions of the domain as river water intrudes and recedes.

[69] The rapid river stage fluctuations modulate seasonal fluctuations resulting in rapid changes in flow to and from the river. Although the cumulative U(VI) flux appears to be a relatively smooth function of time, it actually consists of short segments with zero slope (corresponding to river water flowing inland), separated by an increase in the cumulative flux as the river stage decreases and flow is directed toward the river. The rapid oscillation in river stage gives rise to a seemingly stable linear increase in release of U(VI) whose slope gives the average flux of U(VI) into the river.

[70] Previously, several attempts have been made to estimate the flux of U(VI) to the Columbia River in the field. The *DOE* [1994a] estimated total uranium discharge into the Columbia River from the 300-FF-5 unit as 15 kg/yr. *Fritz and Arntzen* [2007] estimated from field measurements a value of 2.25 μg/m^2/min. Using a surface area of 40,905 m^2 this translates into a rate of approximately 48 kg/yr. Additional work resulted in a revised estimate in surface area of 170,000 m^2 which yields 200 kg/yr. The authors considered this value to overestimate the flux by a factor of 2 due to an overestimate of the surface area and total U(VI) discharge based on the center of the plume.

[71] The flux is expected to vary seasonally with changing conditions such as droughts, Chinook winds, heavy rainfall and other extreme episodic events. The effect of these conditions on the flux could in principle be tested by carrying out simulations with the appropriate river fluctuation event sequence and piecing together the yearly slopes. However, the requisite transient head data for fixing the inland boundary condition that is coincident with these events does not exist.

[72] A comparison of the U(VI) cumulative flux with and without sorption and for different conductance coefficients is shown in Figure 16. It is clear from Figure 16 that the U(VI) flux to the river is highly dependent on the conductance boundary condition.

5.3.3. Nonlabile U(VI) Source Reaction Rate

[73] Shown in Figure 17 is the reaction rate of metatorbernite and the saturation plotted as a function of time for different elevations including the saturated and smear zones at the location of well 399-2-5. As can be seen from the figures strong variations in saturation and reaction rate occur with elevation. These results are sensitive to the equilibrium constant used for metatorbernite. As shown in Figure 17 precipitation occurs at a slow rate close to equilibrium. The calculated flux to the river is sensitive to both the rate constant and equilibrium constant.

[74] The reaction rate for calcite is shown in Figure 18 plotted as a function of time at well 399-2-5. As can be seen from Figure 18, calcite both dissolves and precipitates with changing geochemical conditions as groundwater and river water mix, resulting in a small net dissolution rate of -1.2×10^{-17} mol/cm^3/s.

5.3.4. Relation of Flux to Source Leach Rate

[75] Integrating the transport equation for U(VI) over the entire computational domain provides a global mass balance equation relating the leach rate of U(VI) from sediment to the U(VI) flux at the river boundary. Thus integrating equation (23) over the domain volume V gives

$$\frac{d}{dt}\int_V M_{\mathrm{U(VI)}}(\boldsymbol{r},t)dV = -\int_{\partial V} \boldsymbol{\Omega}_{\mathrm{U(VI)}} \cdot d\boldsymbol{A}, \qquad (46)$$

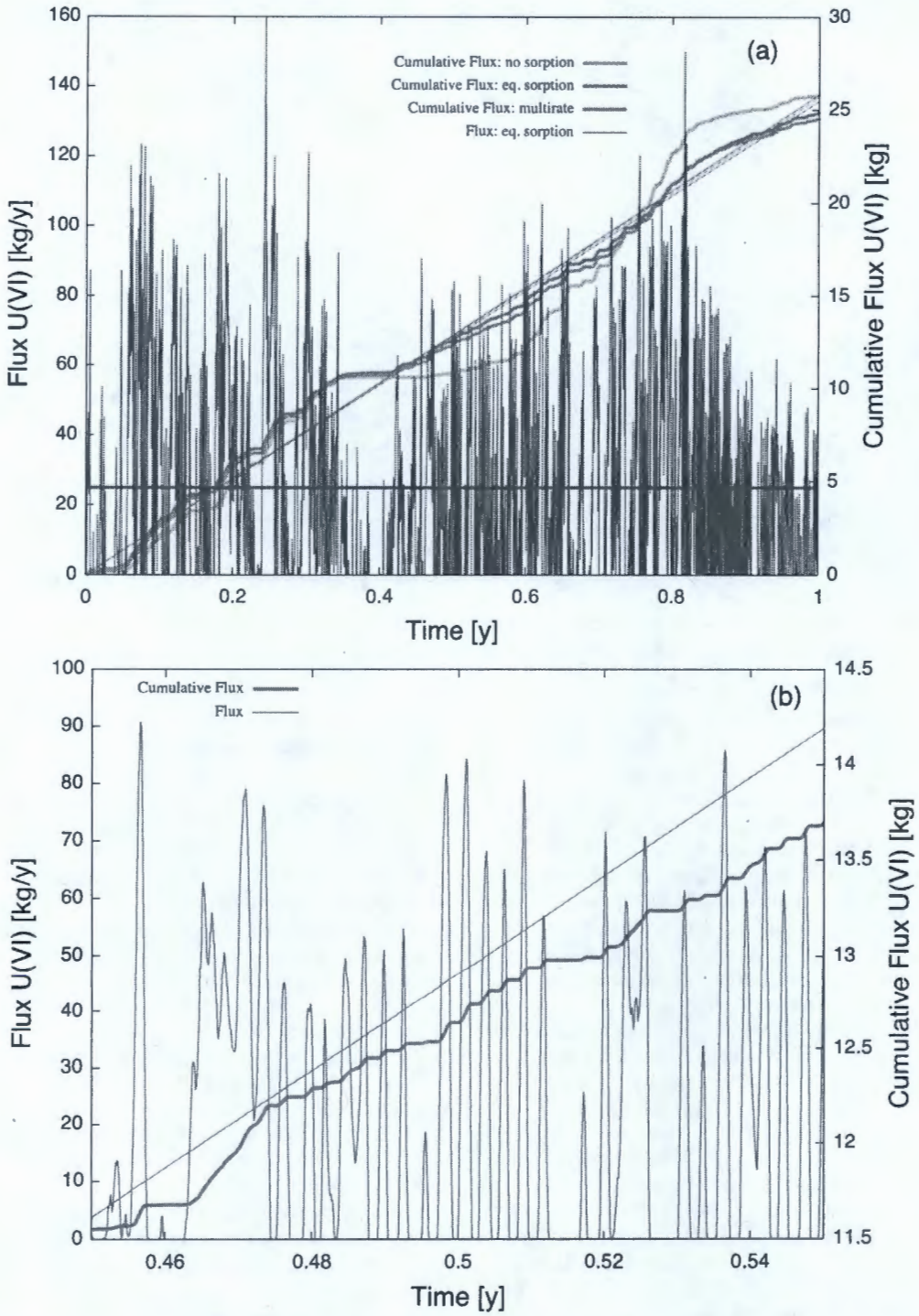

Figure 15. (a) Instantaneous U(VI) flux for equilibrium sorption and cumulative flux for equilibrium and multirate sorption, and no sorption, at the river-aquifer boundary plotted as a function of time using a conductance coefficient of 10^{-12} m. The horizontal line gives a mean flux of 24.89 kg/yr. Also shown is the case with no sorption giving a slope of 25.67 kg/yr. The multirate and equilibrium sorption models give essentially identical results in close agreement to the case without sorption. (b) Magnification of the time interval showing the ratcheting effect of the release of U(VI) into the Columbia River for the equilibrium sorption case shown in Figure 15a.

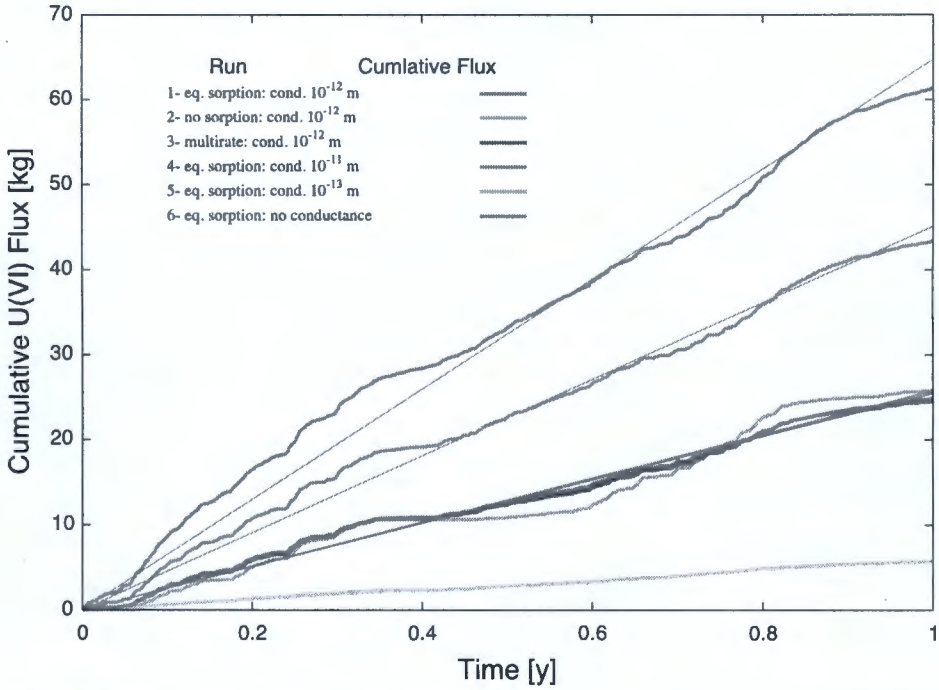

Figure 16. Plot of the U(VI) cumulative flux into the Columbia River with and without sorption and different conductance coefficients C at the river boundary. Mean rates are 64.72 (equilibrium sorption, seepage), 45.16 (equilibrium sorption, $C = 10^{-11}$ m), 25.67 (no sorption, $C = 10^{-12}$ m), 25.47 (equilibrium sorption, $C = 10^{-12}$ m), 25.80 (multirate model, $C = 10^{-12}$ m) kg/yr, and 5.81 (equilibrium sorption, $C = 10^{-13}$ m).

where the total accumulation in moles of U(VI) in the system $M_{\mathrm{U(VI)}}(\boldsymbol{r}, t)$ with contributions from aqueous, sorbed, and mineral forms is given by

$$M_{\mathrm{U(VI)}}(\boldsymbol{r}, t) = \varphi s \Psi_{\mathrm{U(VI)}} + \sum_{\sigma l} S^{\sigma}_{\mathrm{U(VI)},l} + \sum_{m} \nu_{\mathrm{U(VI)},m} \overline{V}_m^{-1} \varphi_m. \tag{47}$$

The integral over the bounding surface ∂V of V appearing on the right-hand side of equation (46) may be assumed to coincide with the aquifer-river boundary because of the low background concentration of U(VI) entering at the inland boundary and the low infiltration rate at the ground surface. To obtain this form for the global mass conservation, the mineral reaction rate I_m was eliminated using equation (27) for the mineral volume fraction and moved to the left-hand side of the equation. Integrating equation (46) over time using equation (44) for the cumulative U(VI) flux then gives approximately

$$\frac{\Delta \mathcal{M}_{\mathrm{U(VI)}}(t)}{\Delta t} = -\overline{F}_{\mathrm{U(VI)}}, \tag{48}$$

where the left-hand side is equal to the mean leach rate with $\mathcal{M}_{\mathrm{U(VI)}}$ equal to the total time averaged inventory of U(VI) at time t

$$\mathcal{M}_{\mathrm{U(VI)}}(t) = \int_V \overline{M}_{\mathrm{U(VI)}}(\boldsymbol{r}, t) dV. \tag{49}$$

Thus the mean flux of U(VI) to the river is balanced by a linear reduction in time of the U(VI) source, as must be the case to conserve mass.

[76] While the absolute mass of U(VI) in the Hanford sediment is unknown, its leach rate can be bounded by measuring the flux of U(VI) into the river. From equation (48), ignoring changes in aqueous and sorptive concentrations, it follows that

$$\overline{F}_{\mathrm{U(VI)}} = -\nu_{\mathrm{U(VI)},\mathrm{mtb}} \int_V \overline{I}_{\mathrm{mtb}} dV. \tag{50}$$

Accordingly, a delicate balance must exist between the leach rate and the flux of U(VI) to the Columbia River. If the flux of U(VI) to the river were to vanish, the leach rate must also vanish because otherwise unrealistic concentrations would build up within the Hanford sediment. Thus the U(VI) leach rate and flux at the river boundary are coupled to one another.

5.3.5. Plume Size Versus Sorption and No Sorption

[77] It is somewhat problematic to compare directly the case without sorption to the cases with sorption because of a noticeable increase in the nonsorbing plume size after the finite time interval of one year (not shown). For the same plume size, the sorbing case would presumably give a somewhat larger flux to the river compared to the case with no sorption. This phenomenon has been observed in preliminary scoping calculations with a larger initial plume. Although counter intuitive, this result can be understood by realizing that retardation keeps U(VI) in place closer to the river bank

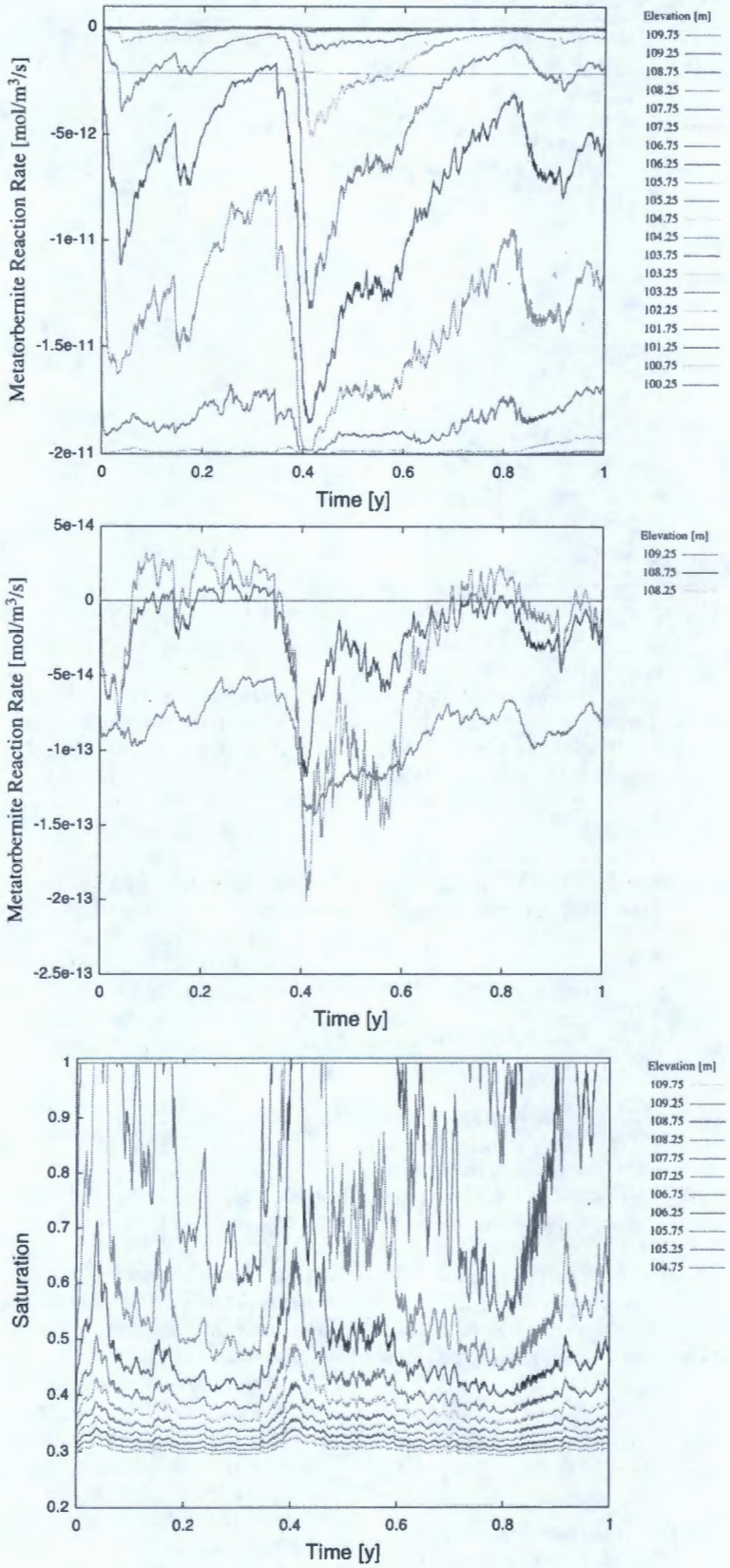

Figure 17. The (top, middle) metatorbernite reaction rate and (bottom) saturation plotted as a function of time at observation well 399-2-5 for different depths including the smear zone and saturated zone for a conductance coefficient of 10^{-12} m. Below the water table the metatorbernite rate is constant, but above the water table it fluctuates as the saturation changes with time and may precipitate (Figure 17, middle).

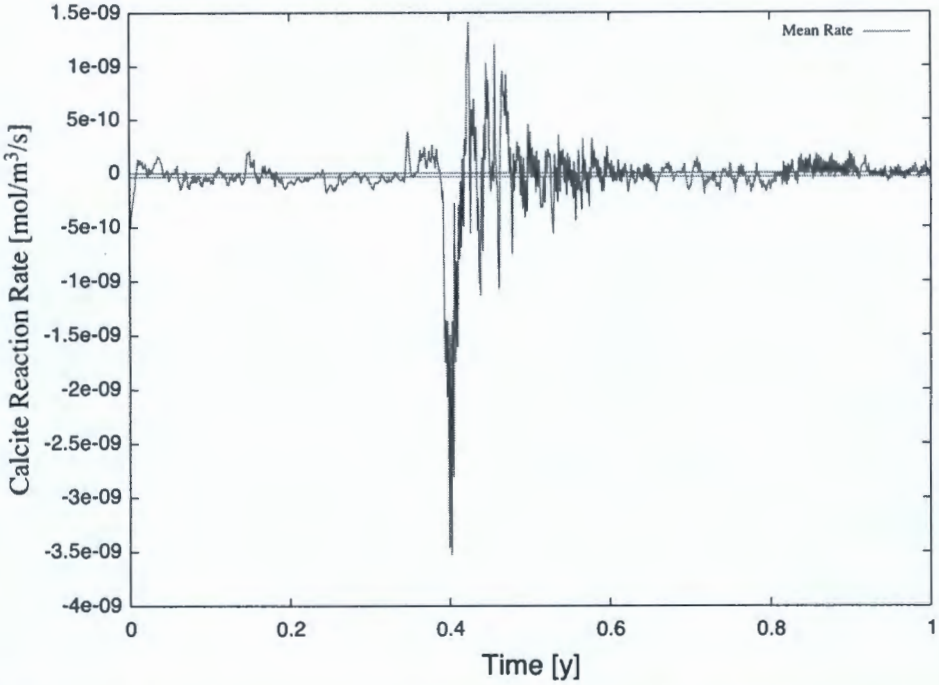

Figure 18. Calcite reaction rate plotted as a function of time at observation well 399-2-5 at a depth of 104 m for a conductance coefficient of 10^{-12} m. Calcite exhibits fluctuations in the rate with a net dissolution.

where it readily leaches into the river during outflow. For the case of no sorption, inflowing river water pushes the plume inland away from the river boundary, resulting in longer periods of reduced flux to the river as the nonsorbing plume must backtrack to the river boundary. The plateau at ~0.4 years in the nonsorbing curve in Figure 15 is indicative of this phenomenon. It will also be noted in Figure 15 that the case without sorption also leads to greater fluctuations about the mean compared to the case with sorption. We hypothesize that the crossover of the nonsorbing case with the sorbing cases at ~0.75 years is caused by an increase in the nonsorbing plume size that results in a larger flux of U(VI) integrated over the river boundary, since visual inspection of the output clearly illustrates the nonsorbing plume increasing in size along the river and the observed total U(VI) concentrations at wells along the river are consistently higher for the sorbing plume. It is likely that this effect could be remedied by carrying out the initialization of the plume to longer times.

5.3.6. Comparison of Sorption in Field and Column Experiments

[78] To better understand the relationship between the model results for the small column experiment, where the multirate sorption model was essential to explain the experimental data, and the field-scale result that showed little difference between sorption and no sorption, a comparison is made between the U(VI) concentrations for the column and field. Figure 19 shows the total U(VI) concentrations as a function of time at well 399-2-1 for the cases of equilibrium sorption, multirate sorption and no sorption with a conductance coefficient of 10^{-12} m. As can be seen from the figure, the U(VI) concentrations for both sorption scenarios are close to one another, consistent with their similar cumulative fluxes to the river. As river water intrudes, desorption takes place tending to buffer the U(VI) concentration. A much wider range of concentrations between equilibrium sorption and no sorption is apparent in the column experiment with unidirectional flow compared to the field case as shown in Figure 4. Thus it is important to take into account oscillating (bidirectional) flow with river and U(VI)-contaminated groundwater at either end of the column in the experiment to realistically mimic the field situation.

5.3.7. Retardation of U(VI)

[79] The local retardation factor $R_{U(VI)}$ for U(VI) is shown in Figure 20 at well 399-2-5 as a function of time. The retardation varies between values of 50 and 120. The higher value occurs as river water infiltrates the region of the well diluting the concentrations of U(VI), carbonate, and pH and thus increasing its retardation. As is clear from Figure 20, retardation depends on the direction of flow to ($q_x > 0$) and from ($q_x < 0$) the river.

[80] As uranium is desorbed it may move with a reduced retardation factor because sorption sites are already equilibrated with uranium, much like a salinity wave in ion exchange processes. Multirate models based on a K_d formulation [*Qafoku et al.*, 2005], although successfully used to fit breakthrough curves from laboratory conducted column experiments, cannot be expected to predict the correct plume behavior under these dynamic conditions.

5.3.8. Effect of Smoothing River Stage Fluctuations

[81] To investigate the influence of smoothing the river stage fluctuations, seven cases were considered of 2 hourly, 3 hourly, 6 hourly, 12 hourly, daily, weekly and monthly averaging in addition to the original hourly. To perform the smoothing a convolution integral was applied to the inland well and river stage data. The smoothed Columbia River

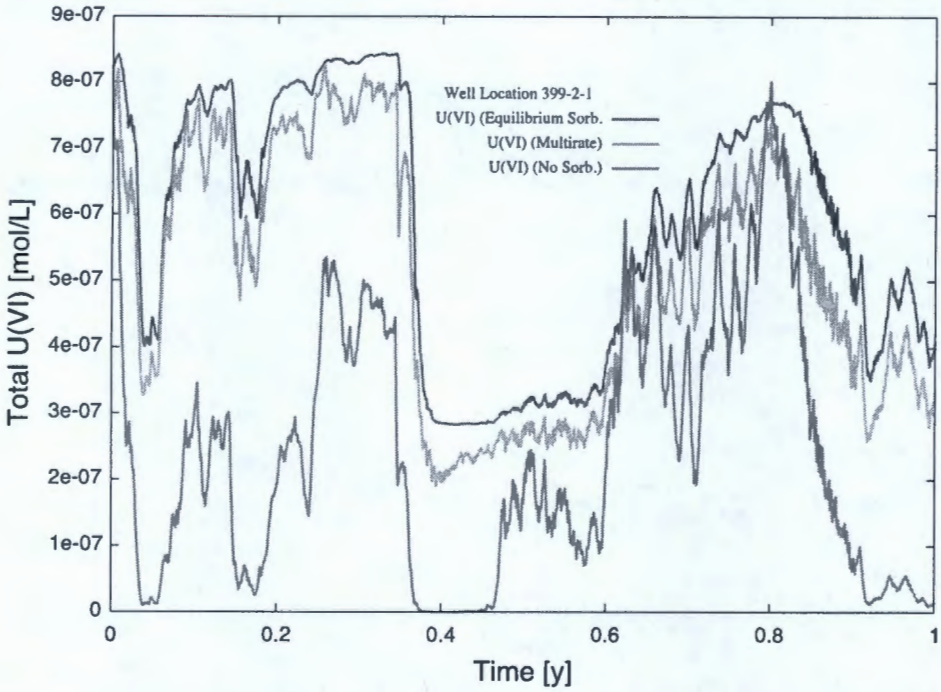

Figure 19. Comparison of U(VI) concentrations at well 399-2-1 at an elevation of 104 m for simulations utilizing equilibrium sorption, multirate sorption, and no sorption with a conductance coefficient of 10^{-12} m. The concentration predicted by the multirate model is approximately bounded by the equilibrium sorption model and no sorption.

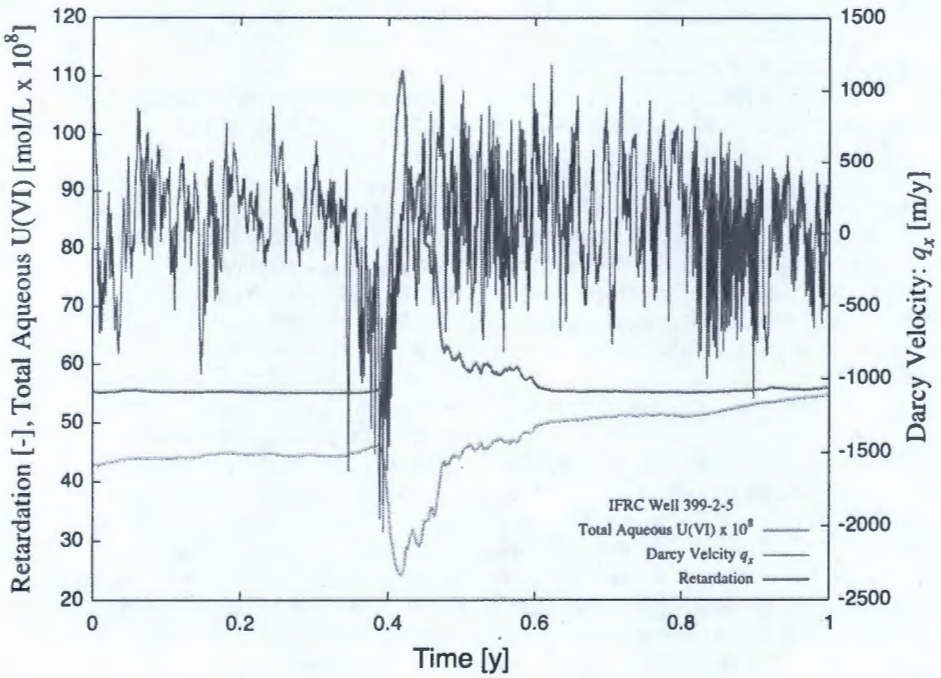

Figure 20. Retardation factor plotted as a function of time at well 399-2-5 for a conductance coefficient of 10^{-12} m showing the correlation with q_x and the total aqueous U(VI) concentration. Positive velocities (i.e., $q_x > 0$) indicate flow to the river.

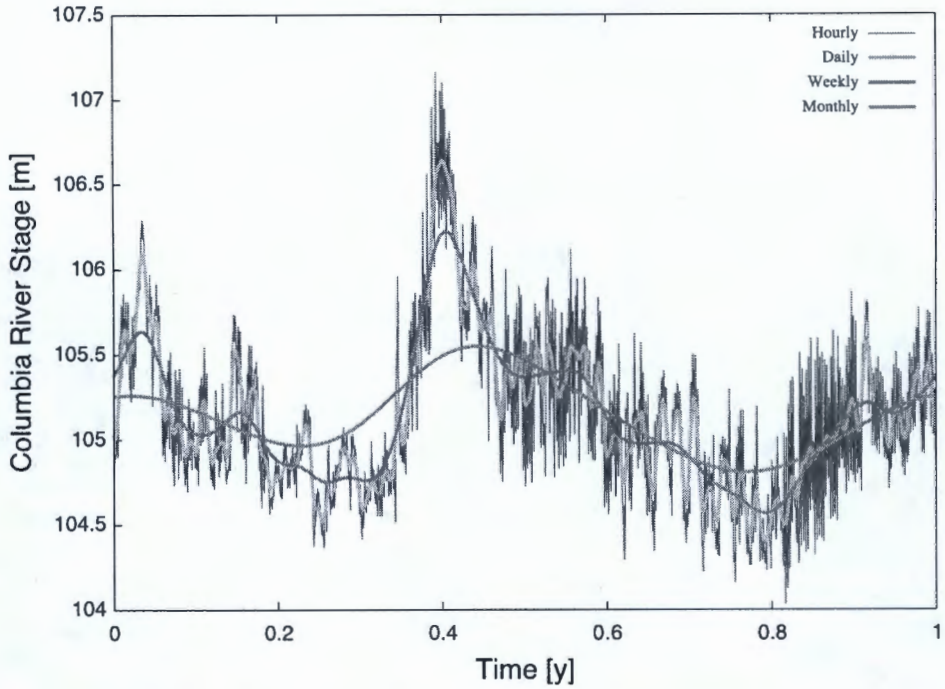

Figure 21. Smoothing of the river stage fluctuations over daily, weekly, and monthly time periods.

data are shown in Figure 21 for hourly, daily, weekly and monthly smoothing intervals. The cumulative flux for U(VI) for all eight cases is compared in Figure 22. In carrying out the simulations the same hourly time step is used in all cases to avoid time truncation errors for comparison purposes. As can be seen from the figure with increased smoothing, the U(VI) flux decreases. As is apparent from the figure, small amounts of smoothing do not significantly alter the slope

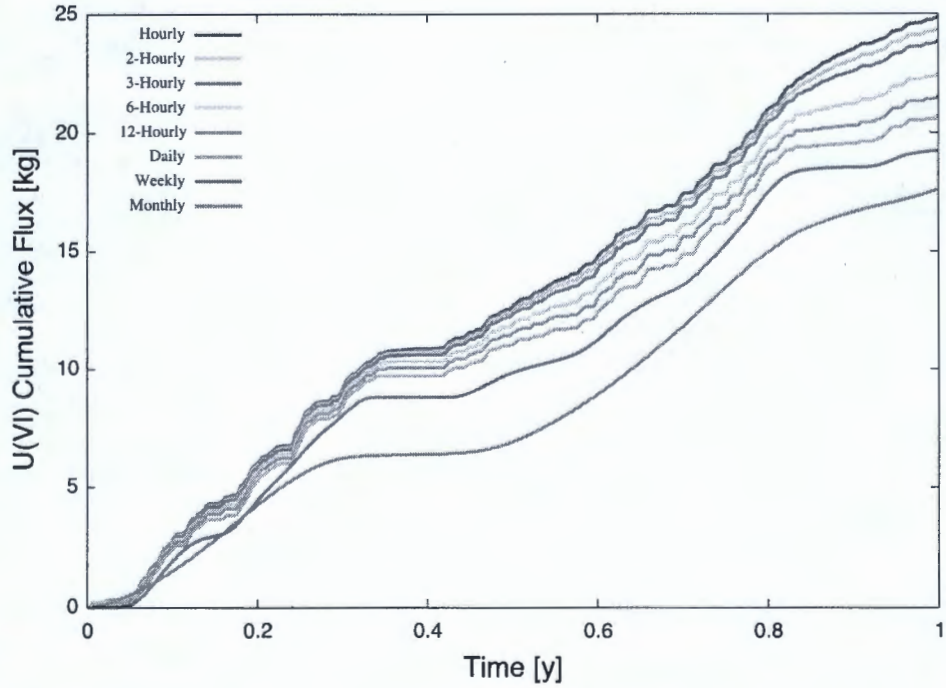

Figure 22. U(VI) cumulative flux for smoothing of the river stage fluctuations over the indicated time periods.

of the cumulative flux and could enable use of larger time steps to carry out calculations over longer time spans, though time step size may be limited by the Courant condition to minimize numerical dispersion.

6. Discussion

[82] Several aspects of the 3-D model deserve further attention.

[83] 1. A 3-D model is essential for capturing the behavior of the U(VI) plume. The 1-D scoping calculation which provided useful information on the contribution of the release rate of U(VI) from the source region to the U(VI) flux to the river, did not account for the release of U(VI) from the vadose zone. A 2-D model in the form of a vertical slice perpendicular to the river, used previously by *Yabusaki et al.* [2008] and *Ma et al.* [2010], is unable to determine the size of the U(VI) plume along the river bank. It is also clear that the flow velocities at the 300 Area are inherently 3-D. At high river stage, flow is predominantly from east to west within the source zone, whereas during low river stage, flow velocities are from the northwest to southeast. Although perhaps difficult to see in Figure 8, the Ringold formation rises in a significant ridge to the south east of the source zone (between source zone and the river). This ridge contributes to the 3-D westerly high-stage and southeasterly low-stage flow.

[84] 2. It is difficult to obtain data for the inland boundaries that coincide with river stage data because of the lack of continuous monitoring at the inland wells. The flow field is sensitive to transient pressure boundary conditions imposed on the sides of the domain. Generally, these boundary conditions must be set by extrapolation of nearby wells. Ultimately it would be desirable to remove the no-flow boundary conditions imposed on the north and south boundaries. To do this, however, would require better characterization of the transient pressure fields at these locations and at the west inland boundary.

[85] 3. It should be emphasized that the only parameters for which direct experimental or field data is not available to constrain, are the river conductance coefficient which is constrained by approximately matching the observed piezometric head, and the effective U(VI) source-term rate for nonlabile U(VI), obtained by adjusting to achieve the maximum observed U(VI) concentration. All other properties such as permeability, porosity, capillary parameters, and sorption parameters were obtained from the literature.

[86] 4. From the results of the 1-D scoping calculations it would appear that the best approach to set up Phase II initial conditions is to run the simulation out sufficiently far in time until the cumulative U(VI) flux to the river stabilizes. The effective rate constant for production of U(VI) from the source region could be adjusted to match the observed flux, but is bounded by the observed maximum concentration in U(VI). Unfortunately, this approach is currently impractical for 3-D simulations because of the long computation times required and the lack of data characterizing the nonlabile U(VI) component. To do so, one would have to utilize an optimization or parameter estimation framework e.g., TAO [*Moré et al.*, 2007].

[87] 5. The best estimate for the U(VI) flux of 25 kg/yr does not include all the U(VI) source contributions at the 300 Area: e.g., NPP, trenches, extended smear zone, etc. Adding additional source regions to the model can only increase the flux, and thus the present value provides a lower bound on the model prediction. Note that the model results are within the range estimated by *Peterson et al.* [2009] of 20–50 kg/yr. Adding the NPP would expect to roughly double the present value obtained for the mean U(VI) flux to the river agreeing with the upper bound derived by *Peterson et al.* [2009]. However, the current model may actually indirectly include some of the other sources to the extent that U(VI) pathways from these regions to the river overlap with the pathway from the SPP. There is no indication that U(VI) is stored in the hyporheic zone [*Fritz and Arntzen*, 2007].

[88] 6. Extrapolations into the future must rely on annual cycling of existing river stage and well head data for the river and inland boundary conditions. Thus the predicted attenuation rate of U(VI) cannot capture details of the river stage fluctuations that occur in the future, although one possibility is construction of a stochastic representation of the river stage including extreme events. However, this would also require deriving transient conditions for the inland boundaries as well.

[89] 7. Given the difficulty in establishing transient boundary conditions for the inland boundaries and the highly heterogeneous nature of the Hanford Unit sediment, it may not be possible to accurately calculate the actual flow velocity at the site. However, this may not be of great concern so long as the qualitative features of the velocity field can be captured in the model and it is possible to compute a realistic U(VI) attenuation rate. As has been demonstrated in this work, much of the oscillatory behavior of the system averages out over time. Recently, *Hammond et al.* [2010] investigated the effects of heterogeneity of the Hanford Unit on the U(VI) flux to the river and found that Gaussian distributions of random permeability based on Hanford IFRC data had very little impact in spite of strong variations in the flow velocity.

7. Conclusion

[90] The main conclusion of this work is that under present-day conditions in which the U(VI) plume at the Hanford 300 Area has evolved from the source region to the Columbia River (Phase II), the U(VI) flux into the river is determined primarily by fluctuations in the river stage combined with a continuous source release of U(VI) feeding the plume. In the model, U(VI) is released both from the saturated and vadose zones through dissolution of nonlabile U(VI) and desorption of labile U(VI). Sorptive processes were found to play a minor role during Phase II on the flux of U(VI) into the Columbia River. In spite of the high-frequency fluctuations in the Columbia River stage, an approximately linear increase in time in the cumulative flux of U(VI) released into the river is obtained in the calculations. A balance is maintained between the rate of leaching and the flux of U(VI) into the river. The model calculations help resolve a long-standing puzzle as to why U(VI) persists over long time spans in the Hanford sediments at concentration levels that exceed EPA standards. By accounting for a nonlabile source of U(VI) it was demonstrated that the prolonged release of U(VI) at the site could be explained through a slow release of nonlabile U(VI) coupled to the undulating water table in the smear zone. The U(VI) leach rate is coupled to the U(VI) flux at

the aquifer-river interface through the affinity term in the transition state rate law.

[91] Central to this work was the use of high-performance computing (HPC) carried out on the world's fastest supercomputer Jaguar, the Cray XT4/XT5 at ORNL. Use of HPC made possible the ability to capture the rapidly fluctuating Columbia River stage and multicomponent U(VI) chemistry including aqueous speciation, sorption through both an equilibrium and multirate model, and mineral dissolution at a sufficiently fine grid resolution to resolve more accurately fluctuations in groundwater velocities in a realistic 3-D domain. The simulations involved approximately 28 million degrees of freedom for multicomponent reactive transport, run on 4096 processor cores, runs that would have required years of computing time on a conventional single processor workstation.

[92] The main findings of this study are as follows:

[93] 1. The flow field, and in particular the river interface (hyporheic zone) modeled through a conductance boundary condition, plays an essential role in controlling the release rate of U(VI) into the Columbia River. The conductance coefficient was adjusted to better match the observed piezometric head at well 399-2-1 yielding a value of 10^{-12} m.

[94] 2. Over the limited simulation time span of 1 year, the U(VI) flux to the Columbia River is predicted to have a mean value of approximately 25 kg/yr in reasonable agreement with field observations of 20–50 kg/yr [*Peterson et al.*, 2009], for a computational domain including the SPP. The peak flux reaches values as high as 160 kg/yr. By measuring the mean U(VI) production rate from nonlabile sources in the field, the model could be further constrained without the necessity of determining the exact chemical form of the nonlabile U(VI). In this regard it must be emphasized that the mean U(VI) leach rate from the nonlabile source is related to the mean U(VI) flux at the river boundary through global mass conservation.

[95] 3. Contrary to expectation, sorption appears to play only a secondary role for Phase II conditions yielding similar results as the case with no sorption. In fact the calculations suggested that sorption should increase the U(VI) flux to the river because of the increased retardation as water flows from the river and reduced retardation as it flows to the river. Perhaps surprisingly, the multirate sorption model showed little difference compared to equilibrium sorption for Phase II conditions, even though it yields significantly different results when applied to unidirectional flow column experiments performed using contaminated Hanford sediments. However, this would be expected because the column experiment did not incorporate bidirectional flow and river water chemistry. It did, however, show a significant difference for Phase III initial conditions for the 1-D scoping calculation. In this regard, it would appear useful to perform a 1-D column experiment with a fluctuating flow rate mimicking the river stage, even though this would not address issues related to U(VI) leaching from the vadose zone.

[96] 4. And lastly, although the river stage fluctuations yield a highly oscillatory flux of U(VI) into the Columbia River, the cumulative flux results in a linear increase in the release of U(VI) with time allowing extrapolation to long time spans and enabling prediction of the time required to remove a given inventory of U(VI). This extrapolation will of course be affected by extreme events such as chinooks and heavy rainfall, for example. However, it can be expected that excursions from the mean behavior will have relatively limited effect in perturbing the general behavior of the system.

Appendix A: Flux of H_2O and U(VI) at the Columbia River

[97] The instantaneous flux of water $F_w(t)$ averaged over the riverbank is calculated using the equation

$$F_w(t) = \int_A d\boldsymbol{A} \cdot \boldsymbol{q}(\boldsymbol{r}, t)\rho_w, \tag{A1}$$

where the surface integral is taken over the river-sediment boundary A. The Darcy volumetric flux at the river boundary, $\boldsymbol{q}(\boldsymbol{r}, t)$, is obtained by solving the 3-D flow equations using Richards approximation for variably saturated conditions. The flux is a rapidly oscillating function of time caused by hourly changes in the river stage. The cumulative flux of water $\mathcal{F}_w(t)$ at the river boundary is equal to the time integral of the flux $F_w(t)$ according to

$$\mathcal{F}_w(t) = \int_{t_1}^{t} dt' \, F_w(t'), \tag{A2}$$

where t_1 is the initial time of integration, taken to be zero or corresponding to a reversal in the direction of mean flow (see Figure 13). It is assumed that between flow reversals the flux F_w can be represented as the sum of its mean value plus a rapidly fluctuating term according to

$$F_w(t) = \overline{F}_w + \delta F_w(t), \tag{A3}$$

where the mean flux $\overline{F}_w$ is computed from the relation

$$\overline{F}_w = \frac{1}{t_2 - t_1} \int_{t_1}^{t_2} dt \, F_w(t). \tag{A4}$$

[98] The time interval (t_1, t_2) over which the mean value is computed corresponds to the time between reversals in the mean flow direction. The fluctuating term δF_w is defined as the difference between the actual flux and its mean

$$\delta F_w(t) = F_w(t) - \overline{F}_w. \tag{A5}$$

[99] The fluctuating part is assumed to average approximately to zero over a time interval Δt according to the equation

$$\int_{\Delta t} dt \, \delta F_w(t) \simeq 0, \tag{A6}$$

where it is assumed that the time interval Δt is large compared to the characteristic time over which river stage fluctuations occur, but small compared to the time between mean flow reversals. With this approximation the cumulative flux is simply a linear function of time

$$\mathcal{F}_w(t) \simeq (t - t_1)\overline{F}_w, \tag{A7}$$

as observed in Figure 13. The instantaneous and cumulative flux for water is shown in Figure 13 over a one year time period. The straight line fits to the cumulative flux between mean flow reversals agree closely with the mean flux over that

time interval, indicating that equation (A6) is an excellent approximation.

[100] Unlike the flux of water which changes sign, the instantaneous U(VI) flux is either positive when the direction of flow is into the river, or zero when flow is in the opposite direction giving rise to a ratcheting effect of release of U(VI). This is because river water contains uranium in negligibly small quantities. Thus the cumulative U(VI) flux can only increase with time or remain the same and the zigzag behavior observed for water with mean reversals in flow direction does not occur for U(VI). Even if the net flux of water is inland, there can still be a net loss of U(VI) to the river. The flux of U(VI) into the Columbia River is computed from the relation

$$F_{\mathrm{U(VI)}}(t) = \int d\boldsymbol{A} \cdot \boldsymbol{q}(\boldsymbol{r},t)\,\Psi_{\mathrm{U(VI)}}, \tag{A8}$$

where the surface integral again is taken over the river boundary, The total cumulative flux given by

$$\mathcal{F}_{\mathrm{U(VI)}}(t) = \int_0^t dt' F_{\mathrm{U(VI)}}(t'). \tag{A9}$$

[101] Since mean reversals in flux do not occur for U(VI), the time integral over the flux begins at $t = 0$. Again, assuming that the U(VI) flux into the river can be separated into mean plus fluctuating terms one has

$$F_{\mathrm{U(VI)}}(t) = \overline{F}_{\mathrm{U(VI)}} + \delta F_{\mathrm{U(VI)}}(t), \tag{A10}$$

with

$$\overline{F}_{\mathrm{U(VI)}} = \frac{1}{T}\int_0^T dt\, F_{\mathrm{U(VI)}}(t), \tag{A11}$$

where the total time interval of interest is denoted by T, and

$$\delta F_{\mathrm{U(VI)}}(t) = F_{\mathrm{U(VI)}}(t) - \overline{F}_{\mathrm{U(VI)}}. \tag{A12}$$

[102] The fluctuating term is assumed to average to zero over sufficiently small time intervals

$$\int_{\Delta t} dt\, \delta F_{\mathrm{U(VI)}}(t) \simeq 0, \tag{A13}$$

so that

$$\mathcal{F}_{\mathrm{U(VI)}}(t) \simeq t\overline{F}_{\mathrm{U(VI)}}. \tag{A14}$$

[103] **Acknowledgments.** We thank three anonymous reviewers who greatly improved the manuscript. This research is supported under the U.S. Department of Energy SciDAC-2 (Scientific Discovery through Advanced Computing) program with funding provided by DOE Offices of Biological and Environmental Research (BER) and Advanced Scientific Computing Research (ASCR). In addition, this research was supported by the Environmental Remediation Sciences Program (ERSP), Office of Biological and Environmental Research (OBER), U.S. Department of Energy, as part of the Hanford 300 Area Integrated Field Research Challenge Project. Supercomputing resources were provided by the DOE Office of Science Innovative and Novel Computational Impact on Theory and Experiment (INCITE) program with allocations on NCCS Jaguar at Oak Ridge National Laboratory.

References

Arai, Y., M. A. Marcus, N. Tamura, J. A. Davis, and J. M. Zachara (2007), Spectroscopic evidence for uranium bearing precipitates in vadose zone sediments at the Hanford 300-area site, *Environ. Sci. Technol.*, *41*, 4633–4639.

Bjornstad, B. N., A. Horner, V. R. Vermeul, D. C. Lanigan, and P. D. Thorne (2009), Borehole completion and conceptual hydrogeologic model for the IFRC well field, 300 Area, Hanford Site—Integrated Field Research Challenge project, *Tech. Rep. PNNL-18340*, Pac. Northwest Natl. Lab., Richland, Wash.

Bond, D. L., J. A. Davis, and J. M. Zachara (2008), Uranium(VI) release from contaminated vadose zone sediments: Estimation of potential contributions from dissolution and desorption, in *Adsorption of Metals by Geomedia II: Variables, Mechanisms, and Model Applications*, edited by M. O. Barnett, and D. B. Kent, pp. 375–416, Elsevier, Amsterdam.

Catalano, J. G., J. P. McKinley, J. M. Zachara, S. Heald, S. C. Smith, and G. Brown Jr. (2006), Changes in uranium speciation through a depth sequence of contaminated Hanford sediments, *Environ. Sci. Technol.*, *40*, 2517–2524.

Davis, J. A., J. A. Coston, D. B. Kent, and C. C. Fuller (1998), Application of the surface complexation concept to complex mineral assemblages, *Environ. Sci. Technol.*, *32*, 2820–2828.

Department of Energy (DOE) (1994a), Phase I remedial investigation report for the 300-FF-5 operable unit, *Rep. DOE/RL-93-21*, Richland Oper. Off., U.S. Dep. of Energy, Richland, Wash.

Department of Energy (DOE) (1994b), Remedial investigation/feasibility study report for the 300-FF-5 operable unit, *Rep. DOE/RL-94-85*, Richland Oper. Off., U.S. Dep. of Energy, Richland, Wash.

Dong, W., and S. C. Brooks (2006), Determination of the formation constants of ternary complexes of uranyl and carbonate with alkaline earth metal (Mg^{2+}, Ca^{2+}, Sr^{2+}, and Ba^{2+}) using anion exchange method, *Environ. Sci. Technol.*, *40*, 4689–4695.

Environmental Protection Agency (1998), U. S. Environmental Protection Agency soil cleanup criteria in 40 CFR Part 192, 20 pp., Washington, D. C.

Fritz, B. G., and E. V. Arntzen (2007), Effect of rapidly changing river stage on uranium flux through the hyporheic zone, *Ground Water*, *45*(6), 753–760.

Fritz, B. G., R. D. Mackley, N. P. Kohn, G. W. Patton, T. J Gilmore, D. P. Mendoza, D. McFarland, A. L. Bunn, and E. V. Arntzen (2007), Investigation of the hyporheic zone at the 300 Area, Hanford site, *Rep. PNNL-16805*, Pac. Northwest Natl. Lab., Richland, Wash.

Guillaumount, R., T. Fanghänet, V. Neck, J. Fuger, D. A. Palmer, I. Grenthe, and M. H. Rand (2003), *Update on the Chemical Thermodynamics of Uranium, Neptunium, Plutonium, Americium and Technetium*, Elsevier, Amsterdam.

Hammond, G. E., P. C. Lichtner, R. T. Mills, and C. Lu (2008), Toward petascale computing in geosciences: Application to the Hanford 300 Area, *J. Phys. Conf. Ser.*, *125*, 012051, doi:10.1088/1742-6596/125/1/012051.

Hammond, G. E., P. C. Lichtner, and M. L. Rockhold (2010), Stochastic simulation of uranium migration at the Hanford 300 Area, *J. Contam. Hydrol.*, doi:10.1016/j.jconhyd.2010.04.005, in press.

Hartman, M. J., L. F. Morasch, and W. D. Webber (2007), Hanford site groundwater monitoring for fiscal year 2006, *Rep. PNNL-16346*, Pac. Northwest Natl. Lab., Richland, Wash.

Ilton, E. S., J. M. Zachara, D. A. Moore, J. P. McKinley, A. D. Eckberg, C. L. Cahill, and A. R. Felmy (2010), A dissolution study of metatorbernite: Thermodynamic properties and the effect of pH and phosphate, *Environ. Sci. Technol.*, in press.

Lichtner, P. C. (1996), Continuum formulation of multicomponent-multiphase reactive transport, in *Reactive Transport in Porous Media*, *Rev. Mineral.*, vol. 34, edited by P. C. Lichtner, C. I. Steefel, and E. H. Oelkers, pp. 1–81, Miner. Soc. of Am., Washington, D. C.

Liu, C., J. M. Zachara, O. Qafoku, J. P. McKinley, S. M. Heald, and Z. Wang (2004), Dissolution of uranyl microprecipitates from subsurface sediments at the Hanford Site, USA, *Geochim. Cosmochim. Acta*, *68*, 4519–4537.

Liu, C., J. M. Zachara, W. Yantansee, P. D. Majors, and J. P. McKinley (2006), Microscopic reactive diffusion of uranium in the contaminated sediments at Hanford, USA, *Water Resour. Res.*, *42*, W12420, doi:10.1029/2006WR005031.

Liu, C., J. M. Zachara, N. P. Qafoku, and Z. Wang (2008), Scale-dependent desorption of uranium from contaminated subsurface sediments, *Water Resour. Res.*, *44*, W08413, doi:10.1029/2007WR006478.

Ma, R., C. Zheng, H. Prommer, J. Greskowiak, C. Liu, J. Zachara, and M. Rockhold (2010), A field-scale reactive transport model for U(VI) migration influenced by coupled multirate mass transfer and surface complexation reactions, *Water Resour. Res.*, *46*, W05509, doi:10.1029/2009WR008168.

McKinley, J. P., J. M. Zachara, C. Liu, and S. M. Heald (2006), Microscale controls on the fate of contaminant uranium in the vadose zone, Hanford Site, Washington, *Geochim. Cosmochim. Acta*, *70*, 1873–1887.

McKinley, J. P., J. M. Zachara, J. Wan, D. E. McCready, and S. M. Heald (2007), Geochemical controls on contaminant uranium in vadose Hanford formation sediments at the 200 area and 300 area, Hanford Site, Washington, *Vadose Zone J.*, *6*, 1004–1017, doi:10.2136/vzj2006.0184.

Moré, J. J., T. S. Munson, and J. Sarich (2007), Optimization in SciDAC applications, *J. Phys. Conf. Ser.*, *78*, 012052, doi:10.1088/1742-6596/78/1/012052.

Peterson, R. E., et al. (2005), Contaminants of potential concern in the 300-FF-5 operable unit: Expanded annual groundwater report for fiscal year 2004, *Rep. PNNL-15127*, Pac. Northwest Natl. Lab., Richland, Wash.

Peterson, R. E., C. F. Brown, and R. J. Serne (2009), Mass balance aspects of persistent uranium contamination in the subsurface at the Hanford Site, Washington, *Rep. PNNL-SA-67979*, Oct. 2009, Pac. Northwest Natl. Lab., Richland, Wash.

Plummer, L. N., and E. Busenberg (1982), The solubilities of calcite, aragonite and vaterite in CO_2-H_2O solutions between 0°C and 90°C, and an evaluation of the aqueous model for the system $CaCO_3$-CO_2-H_2O, *Geochim. Cosmochim. Acta*, *46*, 1011–1040.

Qafoku, N. P., J. M. Zachara, C. Liu, P. L. Gassman, O. Qafoku, and S. Smith (2005), Kinetic desorption and sorption of U(VI) during reactive transport in a contaminated Hanford sediment, *Environ. Sci. Technol.*, *39*, 3157–3165.

Record of Decision (ROD) (1996), Declaration of the record of decision, USDOE Hanford Area 300-FF-1 and 300-FF-5 operable units, Hanford Site, Benton County, Washington, Wash. State Dep. of Ecol., Richland, Wash.

Runchal, A. K., B. Sagar, and N. W. Kline (1992), PORFLO-3: A mathematical model for fluid flow, heat, and mass transport in variably saturated geologic media, users manual, version 1.2, *WHC-EP-0385*, Westinghouse Hanford Co., Richland, Wash.

Sagar, B., and A. K. Runchal (1989), PORFLO-3: A mathematical model for fluid flow, heat and mass transport in variably saturated media—Theory and numerical methods, ver. 1.0, WHC-*EP-0042*, Westinghouse Hanford Co., Richland, Wash.

Singer, D. M., J. M. Zachara, and G. E. Brown Jr. (2009), Uranium speciation as a function of depth in contaminated Hanford Sediments—A micro-XRF, micro-XRD, and micro- and bulk-XAFS study, *Environ. Sci. Technol.*, *43*, 630–636.

Stubbs, J. E., L. A. Veblen, D. C. Elbert, J. M. Zachara, J. A. Davis, and D. R. Veblen (2009), Newly recognized hosts for uranium in the Hanford Site vadose zone, *Geochim. Cosmochim. Acta*, *73*, 1563–1576.

Thorne, P. D., M. P. Bergeron, and V. L. Freedman (2006), Groundwater data package for Hanford assessments, Rev. 1, *Rep. PNNL-14753*, Pac. Northwest Natl. Lab., Richland, Wash.

Williams, B. A., C. F. Brown, W. Um, M. J. Nimmons, R. E. Peterson, B. N. Bjornstad, D. C. Lanigan, R. J. Serne, F. A. Spane, and M. L. Rockhold (2007), Limited field investigation report for uranium contamination in the 300 Area, 300-FF-5 operable unit, Hanford Site, Washington, *Rep. PNNL-16435*, Pac. Northwest Natl. Lab., Richland, Wash.

Williams, M. D., M. L. Rockhold, P. D. Thorne, and Y. Chen (2008), Three-dimensional groundwater models of the 300 Area at the Hanford Site, Washington State, *Rep. PNNL-17708*, Pac. Northwest Natl. Lab., Richland, Wash.

Yabusaki, S. B., Y. Fang, and S. R. Waichler (2008), Building conceptual models of field-scale uranium reactive transport in a dynamic vadose zone-aquifer-river system, *Water Resour. Res.*, *44*, W12403, doi:10.1029/2007WR006617.

Zachara, J. M., J. A. Davis, C. Liu, J. P. McKinley, N. Qafoku, D. M. Wellman, and S. Yabusaki (2005), Uranium geochemistry in vadose zone and aquifer sediments from the 300 Area uranium plume, *Rep. PNNL-15121*, U.S. Dep. of Energy, Washington, D. C.

G. E. Hammond, Energy and Environment Directorate, Hydrology Group, Pacific Northwest National Laboratory, MSIN K9-36, Richland, WA 99352, USA. (glenn.hammond@pnl.gov)

P. C. Lichtner, Earth and Environmental Sciences Division, Los Alamos National Laboratory, EES-16, MSD469, Los Alamos, NM 87545, USA. (lichtner@lanl.gov)